Journal of Medicinal Chemistry

pubs.acs.org/jmc Article

Mapping Chromone-3-Phenylcarboxamide Pharmacophore: *Quid Est Veritas*?

Francesco Mesiti, Alexandra Gaspar,* Daniel Chavarria, Annalisa Maruca, Roberta Rocca, Eva Gil Martins, Sandra Barreiro, Renata Silva, Carlos Fernandes, Sheraz Gul, Oliver Keminer, Stefano Alcaro, and Fernanda Borges*

Cite This: *J. Med. Chem.* 2021, 64, 11169−11182 Read Online

ACCESS | Metrics & More | Article Recommendations | Supporting Information

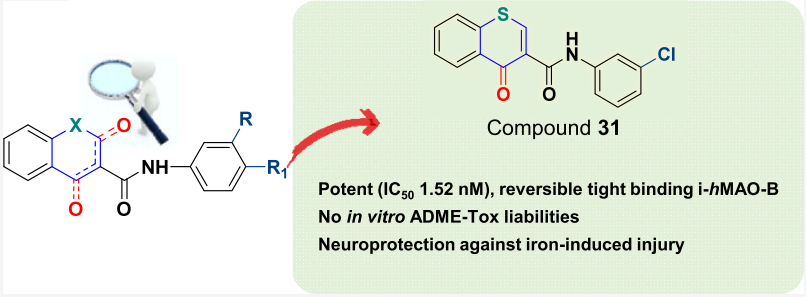

ABSTRACT: Chromone-3-phenylcarboxamides (**Crom-1** and **Crom-2**) were identified as potent, selective, and reversible inhibitors of human monoamine oxidase B (*h*MAO-B). Since they exhibit some absorption, distribution, metabolism, and excretion (ADME)-toxicity liabilities, new derivatives were synthesized to map the chemical structural features that compose the pharmacophore, a process vital for lead optimization. Structure−activity relationship data, supported by molecular docking studies, provided a rationale for the contribution of the heterocycle's rigidity, the carbonyl group, and the benzopyran heteroatom for *h*MAO-B inhibitory activity. From the study, *N*-(3-chlorophenyl)-4*H*-thiochromone-3-carboxamide (**31**) (*h*MAO-B IC_{50} = 1.52 ± 0.15 nM) emerged as a reversible tight binding inhibitor with an improved pharmacological profile. In *in vitro* ADME-toxicity studies, compound **31** showed a safe cytotoxicity profile in Caco-2, SH-SY5Y, HUVEC, HEK-293, and MCF-7 cells, did not present cardiotoxic effects, and did not affect P-gp transport activity. Compound **31** also protected SH-SY5Y cells from iron(III)-induced damage. Collectively, these studies highlighted compound **31** as the first-in-class and a suitable candidate for *in vivo* preclinical investigation.

INTRODUCTION

Human monoamine oxidases A and B (*h*MAO-A and *h*MAO-B, respectively) are mitochondrial flavoenzymes expressed in the brain and peripheral tissues.[1] They catalyze the oxidative deamination of endogenous and dietary monoamines having a pivotal role in regulating the levels of monoamine neurotransmitters.[2] Since *h*MAO-A and *h*MAO-B isoforms exhibit different affinities for specific neurotransmitters, their selective inhibition is considered an attractive approach for the therapy of several neurological disorders.[3] *h*MAO-B is a pharmacological target for the treatment of Parkinson's disease (PD)[3] and has also been described as a potential target for Alzheimer's disease.[4] During aging, the activity and expression of *h*MAO-B are enhanced approximately 4-fold in most of the brain regions.[5] This *h*MAO-B overexpression boosts dopamine (DA) catabolism, with subsequent DA deficiency and generation of hydrogen peroxide and toxic aldehydes, which contribute to increased oxidative stress and neurodegeneration.[5] As such, the use of selective *h*MAO-B inhibitors (i-*h*MAO-B) not only decreases DA catabolism, prolonging its action in the basal ganglia,[3] but also prevents the formation of neurotoxic dopamine-derived oxidative products.[6] The i-*h*MAO-B selegiline and rasagiline are currently used as monotherapy or as add-on therapy to L-DOPA in PD.[7] However, they present adverse effects and safety issues often associated with their irreversible inhibition.[5] Considerable efforts have been made to overcome these drawbacks, which culminated in safinamide approval, the only reversible i-*h*MAO-B in the market.[5] As a result, the discovery of novel reversible i-*h*MAO-B is an active research area in drug discovery, and we report here novel outcomes based on a new scaffold.

Received: March 19, 2021
Published: July 16, 2021

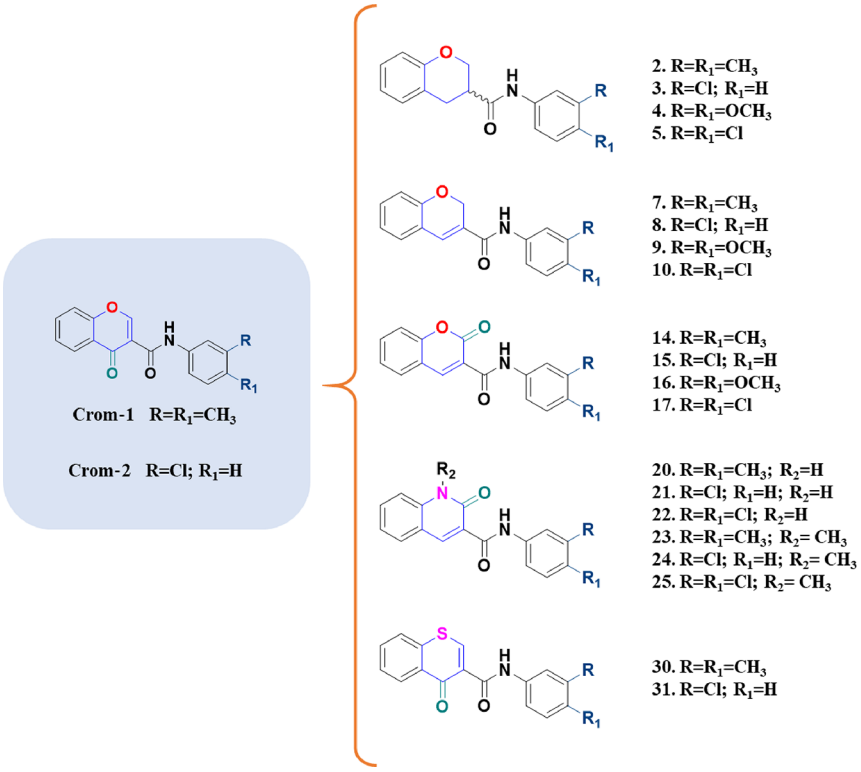

Figure 1. Rational design followed for the mapping of the chromone-3-phenylcarboxamide pharmacophore.

Benzopyrones, such as coumarins and chromones, are considered valid scaffolds for the development of new i-*h*MAO-B.[3,8] Within this framework, benzopyrone-based libraries were developed and screened toward *h*MAOs, and relevant structure−activity relationships (SAR) were established.[9−11] From our preliminary studies, we observed that the location and type of substituent at position C3 of the γ-pyrone nucleus were crucial to obtain potent and selective i-*h*MAO-B.[12] As a result, *N*-(3′,4′-dimethyl phenyl)-4-oxo-4*H*-chromene-3-carboxamide (**Crom-1**, Figure 1) and *N*-(3′-chlorophenyl)-4-oxo-4*H*-chromene-3-carboxamide (**Crom-2**, Figure 1) were identified as the most potent, selective, and reversible i-*h*MAO-B.[10] Notably, the presence of the amide spacer and its direct linkage to the pyrone ring were found to be crucial for *h*MAO-B inhibitory activity. Moreover, the presence of 3,4-dimethyl and 3-chloro substituents at the exocyclic aromatic ring had remarkable effects on the compounds' inhibitory potency against *h*MAO-B.[10,11] Focusing on the lead optimization, we evaluated the effect of substituents located on the aromatic ring of benzopyrone (chromone and its bioisoster coumarin).[11] From this study, we validated chromone-3-phenyl carboxamide as a lead to develop new and reversible i-*h*MAO-B. Then, crystallographic ligand−enzyme studies showed that both **Crom-1** and **Crom-2** occupied the hydrophobic active site of *h*MAO-B.[13] However, despite the promising *h*MAO-B inhibition activity, these compounds presented cytotoxic effects in differentiated SH-SY5Y cells.

The data obtained gave us the rationale to develop selective and potent i-*h*MAO-B based on the chromone-3-phenylcarboxamide pharmacophore with improved absorption, distribution, metabolism, and excretion (ADME)-toxicity properties. To achieve this goal, the first step includes the evaluation of the chemical features that are part of the chromone-3-phenylcarboxamide pharmacophore. We investigated the relevance of key structural features of the benzopyrone moiety on bioactivity, namely, heterocycle rigidity, the presence/absence of a carbonyl group, and the type of heteroatom. Modifications of the substituents at the aromatic exocyclic ring were also explored. Thus, following a rational design strategy (Figure 1), here, we report the synthesis of a novel library and new SAR studies guided by *in silico* and experimental studies. The results were then rationalized using docking studies with crystal structures of *h*MAO-A and *h*MAO-B. The most promising i-*h*MAO-B followed through with preliminary preclinical *in vitro* ADME-toxicity studies, in order to evaluate its cytotoxicity against SH-SY5Y, Caco-2, HEK-293, and MCF-7 cells, cardiotoxicity (*h*ERG inhibition), P-gp modulation, and protection against iron(III)-induced oxidative stress in differentiated neuroblastoma cells. Collectively, these studies allowed the selection of i-*h*MAO-B with the best ADME-toxicity profile suitable for progression to animal studies.

RESULTS AND DISCUSSION

Chemistry. Benzopyran-inspired libraries were obtained following the synthetic strategies depicted in Scheme 1. In accordance with our rational design strategy (Figure 1), compounds lacking the carbonyl group and/or the double bond at the benzopyran ring were synthesized. To assess the relevance of the benzopyran oxygen on the compounds' bioactivity, isosteric replacements by nitrogen and sulfur were also performed. The new derivatives were designed with the same types of substitution patterns of **Crom-1** and **Crom-2** at the phenyl carboxamide ring (3,4-dimethyl and 3-chloro groups, respectively).[10] Additionally, 3,4-dimethoxy and 3,4-dichloro substituents were incorporated at the phenyl exocyclic ring to gather additional SAR data.

Chromane and chromene derivatives (**2**−**5** and **7**−**10**, respectively) were synthetized by a one-pot reaction using

https://doi.org/10.1021/acs.jmedchem.1c00510
J. Med. Chem. 2021, 64, 11169−11182

Scheme 1. Synthetic Strategy Pursued for Synthesis of (A) Chromane-3-phenylcarboxamides (2−5), (B) Chromene-3-phenylcarboxamides (7−10), (C) Coumarin-3-phenylcarboxamides (14−17), (D) 2-Oxoquinoline-3-phenylcarboxamides (20−22) and *N*-Methyl-2-oxoquinoline-3-phenylcarboxamides (23−25), and (E) Thiochromone-3-phenylcarboxamides (30 and 31)[a]

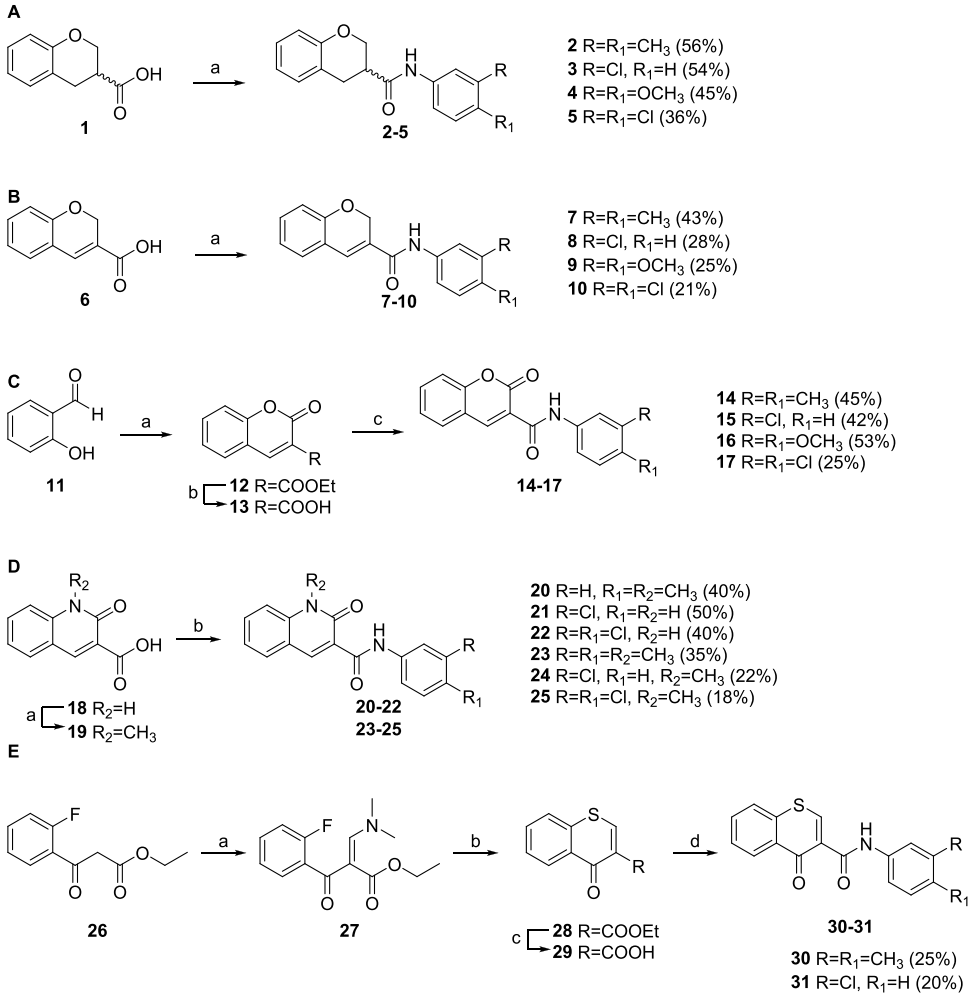

[a]Reagents and conditions: (A,B) (a) $POCl_3$, DMF, appropriate arylamine, rt, 24 h; (C) (a) diethyl malonate, EtOH, pyrimidine, reflux, overnight; (b) NaOH (ethanolic solution), reflux, 1 h; (c) $POCl_3$, DMF, appropriate arylamine, rt, 24 h; (D) (a) CH_3I, K_2CO_3, 60 °C, argon, 1 h; (b) DIPEA, TBTU, appropriate arylamine, rt, 24 h; (E) (a) *N*,*N*-dimethylformamide dimethyl acetal, 115 °C, 1 h; (b) H_2S, −30 °C, 4 h, argon; (c) HCl, AcOH, reflux, 4 h; (d) $POCl_3$, appropriate arylamine, rt, 24 h.

chromane-3-carboxylic (**1**) or chromene-3-carboxylic acids (**6**) as starting materials. The amides were synthesized by an acyl nucleophilic substitution reaction between the appropriate arylamine and the corresponding acyl chloride intermediate, which is generated *in situ* by the addition of phosphoryl chloride ($POCl_3$) (Scheme 1B,A).[10]

Coumarin derivatives (**14**−**17**) were obtained using a three-step synthetic strategy (Scheme 1C). The reaction of salicylaldehyde (**11**) with diethyl malonate afforded coumarin-3-ethyl carboxylate (**12**, Scheme 1C, step a), which, after alkaline hydrolysis, yielded coumarin-3-carboxylic acid (**13**, Scheme 1C, step b).[14] Finally, the $POCl_3$-mediated coupling reaction of **13** with the appropriate arylamine led to the synthesis of coumarin carboxamides (**14**−**17**, Scheme 1C, step c).[10]

The synthetic route used to obtain 2-oxoquinoline derivatives (**20**−**22**) and their *N*-methyl counterparts (**23**−**25**) is outlined in Scheme 1D. First, *N*-methyl-2-oxoquinoline-3-carboxylic acid (**19**) was obtained *via* *N*-methylation of **18** with methyl iodide under alkaline conditions (Scheme 1D, step a).[15] Then, carboxylic acids (**18** or **19**) reacted with the appropriate arylamine, using 2-(1*H*-benzotriazole-1-yl)-1,1,3,3-tetramethylaminium tetrafluoroborate (TBTU) as a coupling agent (Scheme 1D, step b).[16] In this case, the use of $POCl_3$ was not suitable for the synthesis of these amides due to the formation of several byproducts.[17,18]

Thiochromone derivatives (**30** and **31**) were obtained using the synthetic strategy shown in Scheme 1E. The synthesis started with the reaction of ethyl 3-(2-fluorophenyl)-3-oxopropanoate (**26**) with *N*,*N*-dimethylformamide dimethyl acetal affording the intermediate **27** (Scheme 1E, step a), which in turn was reacted with hydrogen sulfide (H_2S) to yield a thiochromone ester (**28**, Scheme 1E, step b).[19] Then, 4-oxothiochromone-3-carboxylic acid (**29**) was synthesized from the hydrolysis of **28** with HCl and acetic acid[20] (Scheme 1E, step c). A coupling reaction of **29** with the appropriate arylamine, in the presence of $POCl_3$, provided thiochromone carboxamides (**30** and **31**, Scheme 1E, step d).[10]

Monoamine Oxidase Inhibition Studies. The evaluation of i-*h*MAOs (**2**−**5**, **7**−**10**, **14**−**17**, **20**−**25**, and **30** and **31**) was performed using a spectrophotometric assay using kynuramine

https://doi.org/10.1021/acs.jmedchem.1c00510
J. Med. Chem. 2021, 64, 11169−11182

Table 1. *h*MAO Inhibitory Activities of Chromane (2−5), Chromene (7−10), Coumarin (14−17), 2-Oxoquinoline (20−22), *N*-Methyl-2-oxoquinoline (23−25), Thiochromone (30 and 31), and Chromone (Crom-1 and Crom-2) Derivatives and Reference Inhibitors[d]

Structure	Compound	R	R_1	IC_{50}±SD (nM)		SI[a]
				*h*MAO-B	*h*MAO-A	
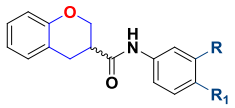	2	CH_3	CH_3	1779±130	19.6%[b]	≥5.62[c]
	3	Cl	H	957±40	10.9%[b]	≥10.44[c]
	4	OCH_3	OCH_3	14.0%[b]	11.8%[b]	—
	5	Cl	Cl	78.8±6.3	16.4%[b]	≥126.90[c]
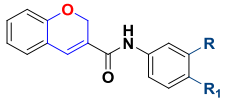	7	CH_3	CH_3	45.7±3.0	13730±2600	300.50
	8	Cl	H	26.4±2.8	11690±4300	443.64
	9	OCH_3	OCH_3	2869±350	20.2%[b]	≥3.48[c]
	10	Cl	Cl	3.16±0.20	4128±1600	1303.03
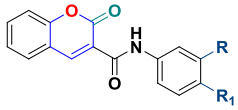	14	CH_3	CH_3	18.8±1.3	26.8%[b]	≥533.33[c]
	15	Cl	H	10.2±1.1	13.5%[b]	≥985.22[c]
	16	OCH_3	OCH_3	*	*	—
	17	Cl	Cl	*	*	—
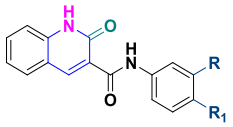	20	CH_3	CH_3	8.1%[b]	1.32%[b]	—
	21	Cl	H	8.9%[b]	2.65%[b]	—
	22	Cl	Cl	*	*	—
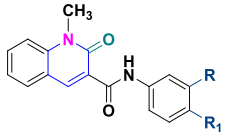	23	CH_3	CH_3	21.10%[b]	7.65%[b]	—
	24	Cl	H	*	*	—
	25	Cl	Cl	*	*	—
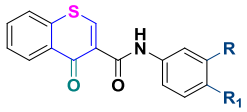	30	CH_3	CH_3	3.35 ± 0.64	0.2%[b]	≥2987.75[c]
	31	Cl	H	1.52±0.15	0.7%[b]	≥6574.62[c]
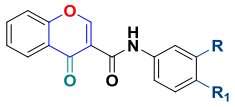	Crom-1	CH_3	CH_3	2.82±0.34	24.2%[b]	≥3539.82[c]
	Crom-2	Cl	H	2.50±0.30	31.4%[b]	≥3913.89[c]
	Rasagiline			45.7±3.0	2340±125	51.21
	Safinamide			25.3±1.8	30.5%[b]	≥395.10[c]
	Clorgyline			2212±264	3.21±0.15	0.0014

[a]SI: *h*MAO-B selectivity index [IC_{50} (*h*MAO-A)/IC_{50} (*h*MAO-B)]. [b]Percentage of inhibition at 10 μM (highest concentration tested). [c]Values obtained under the assumption that the corresponding IC_{50} against *h*MAO-A is the highest concentration tested (10 μM). [d]Asterisks (*) indicate not soluble in phosphate buffer at concentrations higher than 10 μM.

as a substrate and recombinant *h*MAO-A and *h*MAO-B isoforms.[21,22] Since IC_{50} values of **Crom-1** and **Crom-2** reported by Reis *et al.* were determined using the Amplex Red assay,[10] their activity was reassessed under our experimental

https://doi.org/10.1021/acs.jmedchem.1c00510
J. Med. Chem. 2021, 64, 11169−11182

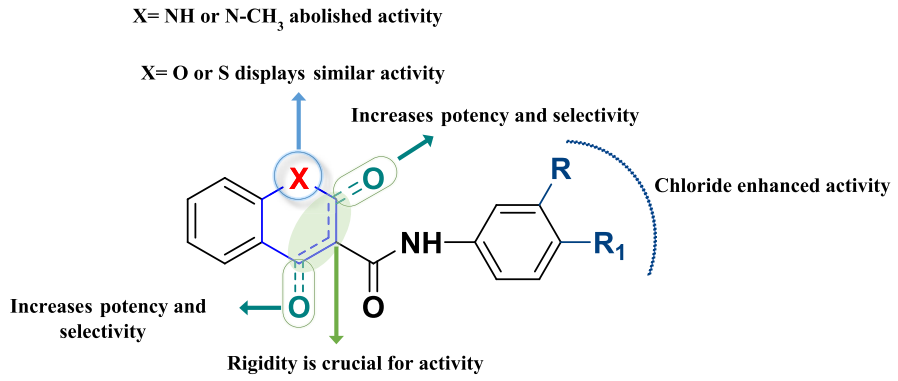

Figure 2. Synopsis of the SAR data obtained in the present work.

conditions. The *h*MAO inhibition potencies (IC_{50} values) and the selectivity index (SI) of the compounds under study and reference inhibitors (rasagiline and safinamide for *h*MAO-B and clorgyline for *h*MAO-A) are presented in Table 1. The results obtained indicate that the novel compounds that exhibited *h*MAO inhibitory activity were more selective toward the isoform B. The *h*MAO-B inhibitory activities of compounds bearing 3-chloro (**3**, **8**, **15**, and **31**) and 3,4-dichloro (**5** and **10**) groups at the exocyclic aromatic ring were, in general, higher than their 3,4-dimethyl counterparts (**2**, **7**, **14**, and **30**) (Table 1). In contrast, the presence of 3,4-dimethoxy substituents decreased (**9**) or even abolished (**4**) *h*MAO-B inhibition at the highest concentration tested (Table 1).

With the exception of **4**, chromane derivatives (**2**, **3**, and **5**) acted as moderate i-*h*MAO-B (**2**, *h*MAO-B IC_{50} = 1779 ± 130 nM; **3**, *h*MAO-B IC_{50} = 957 ± 40 nM; **5**, *h*MAO-B IC_{50} = 78.8 ± 6.3 nM). Since they are considerably less potent than **Crom-1** (*h*MAO-B IC_{50} = 2.82 ± 0.34 nM) and **Crom-2** (*h*MAO-B IC_{50} = 2.50 ± 0.30 nM), we concluded that the absence of the carbonyl group and the double carbon bond led to a remarkable decrease in MAO-B inhibitory activity. In marked contrast, the chromene derivatives (**7**−**10**) were more active toward *h*MAO-B than the chromane counterparts (**7**, *h*MAO-B IC_{50} = 45.7 ± 3.0 nM; **8**, *h*MAO-B IC_{50} = 26.4 ± 2.8 nM; **9**, *h*MAO-B IC_{50} = 2869 ± 350 nM; **10**, *h*MAO-B IC_{50} = 3.16 ± 0.2 nM), demonstrating that benzopyran rigidity is an essential chemical feature for *h*MAO-B inhibition. The compound lacking the carbonyl group but with two chloro substituents in the exocyclic aromatic ring (**10**) was the most potent i-*h*MAO-B of the series.

Subsequently, the effect of the position of the carbonyl group on the pyrone ring (**14**−**17**) on MAOs inhibitory activity was investigated. Coumarins **14** (*h*MAO-B IC_{50} = 18.8 ± 1.3 nM) and **15** (*h*MAO-B IC_{50} = 10.2 ± 1.1 nM) were potent and selective i-*h*MAO-B. Although they were less active than the chromone counterparts (**Crom-1** and **Crom-2**, respectively), they exhibited similar, or even lower, IC_{50} values than the reference i-*h*MAO-Bs safinamide and rasagiline. When compared with chromene derivatives (**7** and **8**), we can conclude that the presence of a carbonyl group at positions C2 (coumarin) or C4 (chromone) improved potency and selectivity. Since the presence of 3,4-dimethoxy substituents was not required for *h*MAO-B inhibition and was associated with poor solubility, this substitution pattern was not considered when designing additional compounds for further studies.

In order to investigate the influence of different heteroatoms on *h*MAO inhibition, 2-oxoquinoline derivatives (**20**−**25**) and thiochromones (**30** and **31**) were synthesized and screened. The 2-oxoquinolines (**20**−**22**) and the *N*-methyl analogues (**23**−**25**) were inactive toward *h*MAOs. The thiochromones (**30** and **31**) displayed *h*MAO-B IC_{50} values within the same concentration range as **Crom-1** and **Crom-2** (**30**, *h*MAO-B IC_{50} = 3.35 ± 0.64 nM; **31**, *h*MAO-B IC_{50} = 1.52 ± 0.15 nM). Overall, the data show that the bioisosteric replacement of O by NH or N−CH_3 atoms at the benzopyrone core results in complete loss of activity and that the amidic tautomerism, which can occur in the 2-oxoquinoline-based compounds, does not influence the *h*MAOs inhibition properties. A recent work on 4-hydroxyquinoline and *h*MAOs reveals important findings that also supported the data.[17] In marked contrast, O to S isosteric replacement was well-tolerated leading to potent and selective i-*h*MAO-B. Of note, the thiochromone amide (**31**) was the most potent i-*h*MAO-B, showing an IC_{50} value lower than safinamide and the parent chromones (**Crom-1** and **Crom-2**). Taking these data together, the results obtained enabled the establishment of robust SAR that is summarized in Figure 2.

Evaluation of the Enzyme−Ligand Inhibition Mechanism. To further evaluate the type of binding between *h*MAO-B and the most potent i-*h*MAO-B (**31**), time-dependent inhibition studies were performed. The reference irreversible (rasagiline) and reversible (safinamide) i-*h*MAO-Bs were also included in these experiments (Figure 3). The data obtained with rasagiline showed a decay in the residual enzyme activity after 30 min incubation, which is consistent with irreversible *h*MAO-B inhibition. In contrast, the results obtained with safinamide showed an increase in *h*MAO-B activity over time indicating

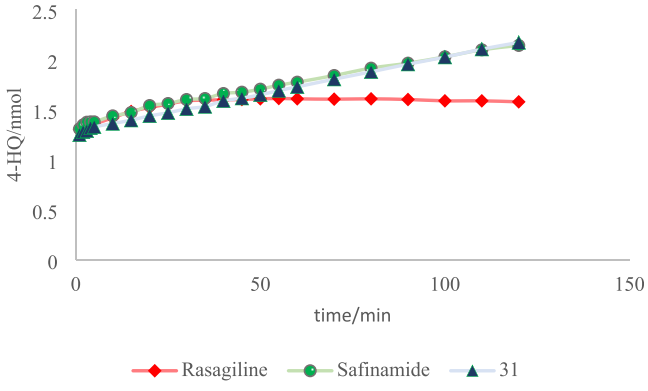

Figure 3. Time-dependent enzyme inhibition studies for rasagiline, safinamide, and compound **31**. Enzymatic activity is expressed in the amount of 4-hydroxyquinoline (4-HQ, nmol). Data are the mean ± SD of three different experiments.

https://doi.org/10.1021/acs.jmedchem.1c00510
J. Med. Chem. 2021, 64, 11169−11182

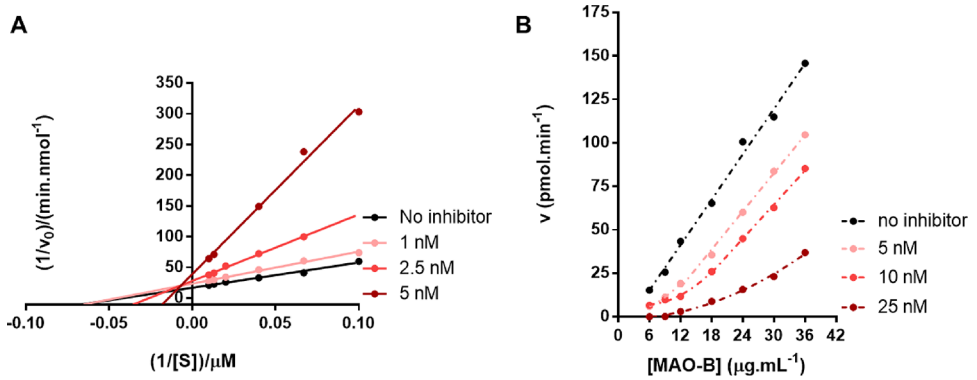

Figure 4. (A) Double reciprocal plot of the initial velocity of *h*MAO-B at increasing substrate concentrations (10−100 μM) in the absence or the presence of compound **31**. (B) Effect of total enzyme concentration on *h*MAO-B inhibition by compound **31** (Ackermann−Potter plot).

reversible inhibition. Compound **31** exhibited an inhibition profile similar to safinamide, suggesting that it acts as a reversible i-*h*MAO-B. The reversible inhibition mechanism could minimize the adverse effects and safety issues often associated to irreversible i-*h*MAO-B.

Moreover, to clarify the inhibition mechanism of the most potent i-*h*MAO-B (**31**), kinetic experiments were performed. The assay was carried out by measuring the initial rates of the *h*MAO-B activity at six different concentrations of kynuramine (substrate) in the absence or presence of three different concentrations of compound **31**. The kinetic parameters of the Michaelis−Menten reaction were analyzed using a double reciprocal Lineweaver−Burk plot, which provides a better visual assessment of enzyme inhibition data. As reported in Figure 4A, the data were fitted to lines intersecting in the upper-left quadrant of the Lineweaver−Burk plot indicating a mixed-type inhibition mechanism.

Since this type of behavior can be indicative of "tight binding inhibition",[23,24] the kinetics was additionally investigated by using seven different *h*MAO-B concentrations in the absence or presence of three different concentrations of compound **31** (SI). The Ackermann−Potter plot (Figure 4B) clearly resulted in asymptotic concave curves showing that compound **31** is a tight binding inhibitor.

These results were in line with our previous findings and strengthen the concept that mixed-type inhibition behavior may occur when compounds bind to the enzyme active site in a "tight binding inhibition" manner.[10,13]

Molecular Ligand−Enzyme Studies. Following the *in vitro* studies, molecular modeling studies were carried out for the best benzopyran-based i-*h*MAO-B to better explore the *in silico* ligand−target interactions. Moreover, the binding mode of the selected compounds on *h*MAO-A was studied to define their strong *h*MAO-B selectivity. In the case of the chromane derivatives (**2**, **3**, and **5**), both enantiomers *R* and *S* were explored. The best thermodynamic complex, provided by the application of the XP Glide protocol and by further thermodynamic characterization through the MM-GBSA (ΔG_{bind}), was analyzed. Coulomb (coul) and van der Waals (vdW) components were also examined to evaluate the nonbonded interaction energy contribution (Table S1, SI).

In general, the data analysis showed good target−ligand interactions. However, the theoretical binding energies, considered as ΔG_{bind}, did not perfectly match with the IC_{50} values obtained since in these calculations, translational, rotational, and vibrational entropy changes were ignored. However, it is interesting to observe that for each series, the most active compound also showed the best ΔG_{bind}. Overall, the *in silico* prediction studies are in line with the selectivity of the compounds toward the *h*MAO-B isoform than *h*MAO-A (Table S1, SI). In particular, the vdW component strongly favored *h*MAO-B binding when compared to *h*MAO-A (Table S1, SI). Chromane (**2**, **3**, and **5**), chromene (**7**−**10**), coumarin (**14** and **15**), and thiochromone (**30** and **31**) derivatives shared a similar docking profile into the *h*MAO-B binding pocket, with their heterocycle facing FAD. The binding mode of the most potent compounds for each series (Figure 5) is characterized by the establishment of an H-bond with the side chain of Tyr435 and several hydrophobic interactions with Tyr398, Tyr60, Gln206, Leu171, Ile199, Leu164, Leu167, and Phe168, as observed in the crystal structure of **Crom-2** (Figure S1B). For the chromane enantiomers *R*/*S*, an overlapping binding mode toward *h*MAO-B was observed (Figure 5A,B and Figure S2, SI), except for the enantiomer *S* of **2** (Figure S2C, SI), which showed the flipped chromane ring by preventing the H-bond with Tyr435. Interestingly, both enantiomers of the most active chromane derivative (**5**) engage an additional halogen bond with Pro102 (Figure 5A,B).

In accordance with the biological results, chromene derivatives showed several favorable interactions due to the double bond present at C3-C4, endowing them with higher planarity and leading to a better orientation in the *h*MAO-B binding site (Figure 5C and Figure S3, SI). Moreover, **7** (Figure S3A, SI) and **9** (Figure S3C, SI), the two low-potency molecules of the series, lose the H-bond with Tyr435 due to the inverted position of the chromene ring. Interestingly, the binding mode of **10**, the most active compound of this series, is favored by the presence of the chlorine in *meta*, which establishes a halogen bond with Pro102 (Figure 5C) as observed for **5**.

Regarding the coumarin series, the best docking poses of **15** established a further $\pi-\pi$ interaction with Phe343, by means of the aromatic portion of the coumarin ring (Figure 5D). Moreover, it was observed that the two methyl groups of derivative **14** interact with the hydrophobic pocket created by several residues, such as Phe168, Leu167, Ile316, Trp119, Leu164, Pro104, Phe103, Pro102, Ile199, and Ile198 (Figure S4A, SI), while **15** places the *meta*-chlorine similarly to **Crom-2** in its crystal structure (Figure 5D and Figure S1B).

Finally, the thiochromone derivatives, **30** and **31**, perfectly fit the hydrophobic flat active site of the *h*MAO-B. Both complexes exhibited an H-bond between the carbonyl group of the thiochromone ring and the side chain of Tyr435, and the most

https://doi.org/10.1021/acs.jmedchem.1c00510
J. Med. Chem. 2021, 64, 11169−11182

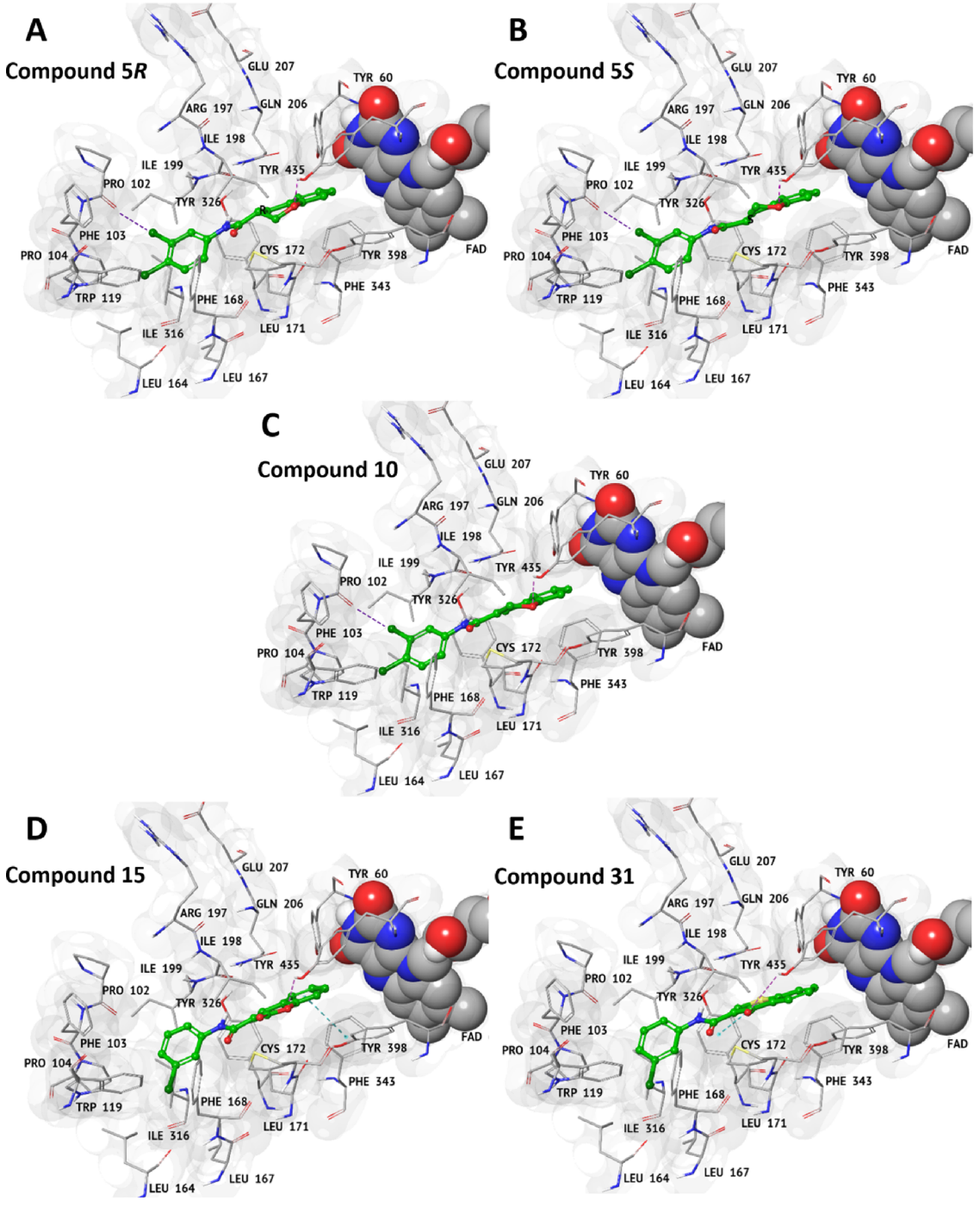

Figure 5. Best docking pose of the most active compounds for each series (A) **5*R***, (B) **5*S***, (C) **10**, (D) **15**, and (E) **31** against *h*MAO-B. Ligands are shown in green carbon ball-and-sticks, while the protein is represented as a gray surface and FAD in CPK. H-bonds, halogen, and $\pi-\pi$ interactions are displayed as dashed purple, violet, and cyan lines, respectively. Amino acid residues involved in the molecular interactions are shown as gray carbon sticks.

active compound **31** engages a further $\pi-\pi$ interaction with Tyr326 and places the *meta*-chlorine similarly to **Crom-2** (Figure 5E and Figure S1B, SI). As previously reported, docking results on *h*MAO-A are reported in the Supporting Information (Figures S5−S8, SI).

Furthermore, the pan-assay interference compound (PAINS) *in silico* assay was run for the compounds studied, using two different methods, namely, ZINC PAINS Pattern Identifier and False Positive Remover tools. The analysis of the results obtained indicated that the chromone (**2**, **3**, and **5**) chromene (**7**−**10**), coumarin (**14** and **15**), and thiochromone (**30** and **31**) derivatives were not potential PAINS.

Furthermore, we estimated the drug-like properties of **Crom-1**, **Crom-2**, and the most potent derivatives (**10**, **15**, **30**, and **31**) to predict their capability to reach the central nervous system (CNS). The drug-like properties were studied by estimating some important physicochemical parameters including the molecular weight (MW), topological polar surface area (tPSA in Å^2), number of hydrogen bond acceptors (HBA), number of hydrogen bond donors (HBD), and number of rotatable bonds

https://doi.org/10.1021/acs.jmedchem.1c00510
J. Med. Chem. 2021, 64, 11169−11182

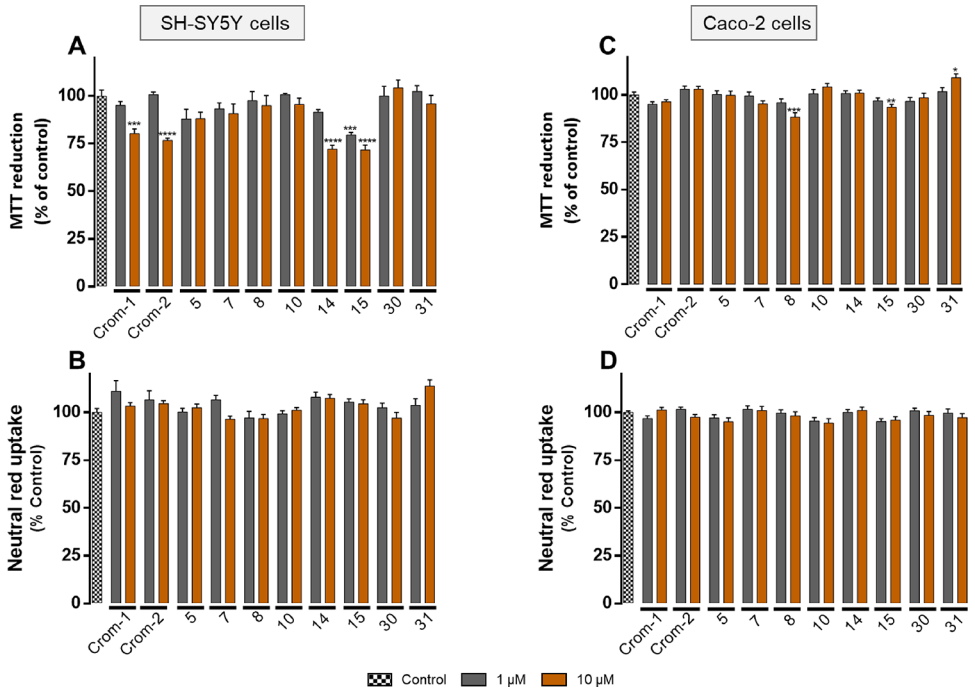

Figure 6. Cellular viability of differentiated SH-SY5Y (A,B) and Caco-2 cells (C,D) following treatment with **Crom-1**, **Crom-2**, and compounds **5**, **7**, **8**, **10**, **14**, **15**, **30**, and **31** at 1 (black) and 10 μM (orange) for 24 h. Cytotoxicity was evaluated by measuring metabolic (A,C) and lysosomal activities (B,D) using MTT reduction and NR uptake assays, respectively. Results are expressed as mean ± SEM from at least three independent experiments, performed in triplicate. Statistical comparisons were performed by one-way ANOVA (A,B) and by Kruskal–Wallis test (C,D). In all cases, p values lower than 0.05 were considered significant (*$p < 0.05$, **$p < 0.01$, ***$p < 0.001$, and ****$p < 0.0001$ vs untreated cells).

(RB). Overall, the values obtained were in line with the general drug-likeness requirements of the CNS-active drugs (Table S2, SI). An important physicochemical parameter used to estimate the ability of a compound to cross the blood–brain barrier (BBB) by passive diffusion is the logarithm of the ratio of the compound concentration in the brain and in blood (log BB). It was reported that compounds with log BB < −1 are unlikely to act as CNS drugs due to their low distribution into the brain.[25] The compounds under study showed log BB values suggesting > −1, indicating that these derivatives may cross the BBB and reach the CNS (Table S2, SI). It is important to note that based on the predicted tPSA and log BB values, the thiochromone **31** is more likely to cross the BBB than **Crom-2**.

Preliminary *In Vitro* Preclinical ADME-Toxicity Studies. Following the discovery of novel, potent, and selective benzopyran-based i-*h*MAO-B, preliminary *in vitro* preclinical ADME-toxicity studies were performed. These included the evaluation of the compounds' cytotoxicity against SH-SY5Y, Caco-2, HUVEC, HEK-293, and MCF-7 cells, cardiotoxicity (*h*ERG inhibition), P-gp modulation, and protection against iron(III)-induced oxidative stress.

Cytotoxicity Studies in SH-SY5Y and Caco-2 Cells. The cytotoxicity profile of the most promising i-*h*MAO-B (*h*MAO-B IC_{50} < 80 nM) was assessed in differentiated neuroblastoma (SH-SY5Y) and in colon adenocarcinoma (Caco-2) cells, two cell lines extensively used to assess the safety of drug candidates.[26,27] Prior to conducting the cytotoxicity experiments with the test compounds, SH-SY5Y cells were treated with differentiation-inducing agents to obtain cells morphologically similar to dopaminergic neurons.[28] Since the clinical symptoms of PD result mainly from the loss of dopaminergic neurons, differentiated SH-SY5Y cells are a suitable cellular model to evaluate the neurotoxicity profile of drug candidates for PD.[29]

Differentiated SH-SY5Y cells and Caco-2 cells were treated with two different concentrations (1 and 10 μM) of compounds **5**, **7**, **8**, **10**, **14**, **15**, **30**, and **31** for 24 h. **Crom-1** and **Crom-2** were also included in these experiments for the establishment of structure–toxicity relationships (STR). Cellular cytotoxicity was determined using the methylthiazolyldiphenyltetrazolium bromide (MTT) reduction assay and the neutral red (NR) uptake assay. The MTT assay is based on the reduction of MTT into the respective formazan by metabolically active cells,[30] while the NR uptake assay is based on the lysosomal accumulation of the NR dye in living cells.[31] The results obtained showed that treatment of differentiated SH-SY5Y cells with **Crom-1**, **Crom-2**, and compound **14** at 10 μM led to a marked decrease in MTT reduction (% MTT reduction was <85%) (Figure 6A). Compound **15** also significantly decreased MTT reduction in neuroblastoma cells at 1 (79.5%) and 10 μM (71.8%) (Figure 6A). In contrast, incubation of differentiated SH-SY5Y cells for 24 h with compounds at both concentrations did not significantly affect NR uptake (Figure 6B). In Caco-2 cells, only compounds **8** (88.3%) and **15** (93.5%), at 10 μM, slightly decreased the cellular metabolic activity (Figure 6C) without any effect on lysosomal activity. The treatment with the other compounds did not affect MTT reduction (Figure 6C) and NR uptake (Figure 6D) when compared with control cells.

Overall, the data obtained indicate that chromones **Crom-1** and **Crom-2** and coumarins **14** and **15** negatively affected cellular metabolic activity of differentiated SH-SY5Y cells. In contrast, chromane derivative **5**, chromene derivatives **7**, **8**, and **10**, and thiochromones **30** and **31** did not induce significant cytotoxic effects in both differentiated SH-SY5Y cells and Caco-2 cells, exhibiting a broader safety window than **Crom-1** and **Crom-2**. Based on these preliminary results, we can conclude that despite the slight improvement of *h*MAO-B inhibition

https://doi.org/10.1021/acs.jmedchem.1c00510
J. Med. Chem. 2021, 64, 11169–11182

Table 2. Preliminary Preclinical *In Vitro* ADME-Toxicity Studies: Cytotoxicity in a Panel of Cell Lines (HUVEC, HEK-293, and MCF-7) for 24 h and Cardiotoxicity (*h*ERG Inhibition) for Crom-1, Crom-2, 10, and 31

	% cytotoxicity at 10 μM			cytotoxicity IC_{50} (μM)			% inhibition at 10 μM
compound	HUVEC	HEK-293	MCF-7	HUVEC	HEK-293	MCF-7	*h*ERG
10	64.4 ± 10	<10	<10	8.4 ± 2.5	inactive	inactive	<10
31	<10	<10	<10	inactive	inactive	inactive	<10
Crom-1	<10	<10	<10	inactive	inactive	inactive	<10
Crom-2	<10	<10	<10	inactive	inactive	inactive	<10

properties, the presence of a carbonyl group in the benzopyran scaffold at positions C4 (chromones) or C2 (coumarins) of the heterocyclic ring was associated with increased cytotoxicity. However, thiochromones **30** and **31** with a carbonyl group at position C4 did not show significant cytotoxicity effects in both cellular models.

Cytotoxicity Studies in HUVEC, HEK-293, and MCF-7 Cells and Cardiotoxicity (*h*ERG Inhibition). The two most active compounds (**10**, *h*MAO-B IC_{50} = 3.16 ± 0.2 nM and **31**, *h*MAO-B IC_{50} = 1.52 ± 0.15 nM) and the parent chromones (**Crom-1** and **Crom-2**) were then selected for the evaluation of their cytotoxicity in a panel of cell lines (HUVEC, HEK-293, and MCF-7). Cells were treated with the test compounds at 10 μM for 24 h exposure, and the cellular cytotoxicity was evaluated using previously described methods.[26,32] Briefly, cellular cytotoxicity was determined in triplicate using a highly sensitive luminescence-based commercial kit that measures intracellular ATP levels (Promega). In general, negligible cytotoxic effects were observed in all cell lines (<10% inhibition at 10 μM) (Table 2). The only exception was compound **10**, which was associated with moderate toxicity in HUVEC cells (cellular cytotoxicity at 10 μM, 64.4 ± 10%; cytotoxicity IC_{50}, 8.4 ± 2.5 μM).

Compounds were also tested for potential cardiotoxicity using the predictor *h*ERG fluorescence polarization (FP) binding assay (Thermo). The assay relies on the use of a homogenized membrane solution containing *h*ERG, which, in the presence of a fluorescent tracer, yields a high FP signal. If compounds displace the fluorescent tracer, then a reduction in the FP signal indicating *h*ERG inhibition is observed. In the case of **Crom-1**, **Crom-2**, **10**, and **31**, negligible *h*ERG inhibition at 10 μM was observed (<10% inhibition) (Table 2).

Evaluation of P-glycoprotein (P-gp) Transport Activity. One of the main challenges for an effective drug transport to the brain is the blood−brain barrier (BBB), the main interface between the brain and the circulatory system.[33] The BBB restricts the permeability of CNS drugs,[34] a problem that is partially linked to the presence of efflux pumps such as the P-gp at the luminal membrane of brain capillary endothelial cells.[35] The P-gp uses adenosine triphosphate (ATP) to actively extrude a wide variety of lipophilic drugs against their concentration gradient,[36] contributing to the high attrition observed for CNS drugs and drug candidates.[37] Caco-2 cells have been accepted as a useful *in vitro* model to evaluate BBB drug permeability and P-gp-mediated transport.[36] Therefore, in this study, we evaluated the P-gp modulatory activity of compounds **10** and **31** and the reference chromones **Crom-1** and **Crom-2**. The assay was performed in Caco-2 cells using Rhodamine 123 (RHO 123), a P-gp substrate, and zosuquidar, a specific third-generation P-gp inhibitor.[30] Overall, the pretreatment of Caco-2 cells with the selected i-*h*MAO-B at 10 μM did not significantly affect P-gp transport activity (Figure 7).

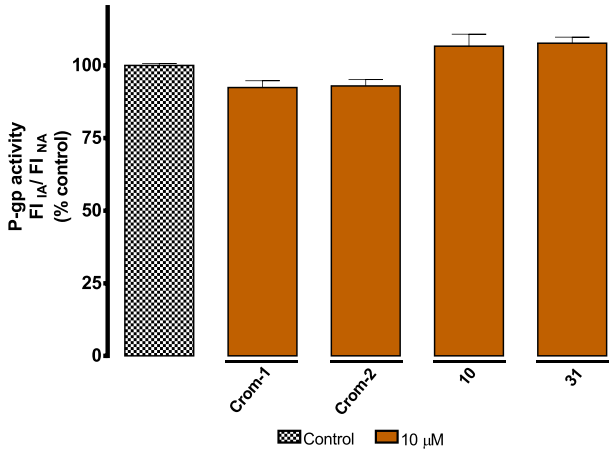

Figure 7. Evaluation of P-gp activity by fluorescence spectroscopy in Caco-2 cells exposed to **Crom-1**, **Crom-2**, and compounds **10** and **31** (10 μM) during the incubation period with the fluorescent substrate (RHO 123, 5 μM). Results are presented as mean ± SEM from at least three independent experiments, performed in triplicate. Statistical comparisons were performed by one-way ANOVA.

Protection against Iron(III)-Induced Damage in Neuroblastoma Cells. The association between iron and PD is long-standing since daily exposure to elevated iron levels is a risk factor for the development of this neurodegenerative disease.[38] In fact, the development of new multitarget compounds that can chelate iron and prevent ferroptosis is one of the strategies currently used to develop new drug candidates for PD. With this in mind, we evaluated whether **Crom-1**, **Crom-2**, and compounds **10** and **31** can protect differentiated SH-SY5Y cells against iron(III)-induced damage. After a pretreatment with the test compounds at 1 and 10 μM for 30 min, cells were treated with iron(III) at 1000 and 1500 μM for 24 h. Cellular cytotoxicity was measured using the NR uptake assay. The results obtained are shown in Figure 8.

Compared with nontreated cells, the 24 h treatments with only iron(III) at 1000 and 1500 μM reduced 55.7 ± 5.8% and 44.9 ± 4.4% of cellular lysosomal activity, respectively. As shown in Figure 8, when cells were coincubated with iron(III) at 1000 μM, no significant protection was observed for the compounds **Crom-1**, **Crom-2**, and **10**. Remarkably, a moderate but significant increase in lysosomal activity was observed in cells pretreated with compound **31** at 10 μM (63.0 ± 7.0%, $p < 0.01$). No significant protection was observed when cells were coincubated with i-*h*MAO-B and iron(III) at 1500 μM. Together with the data obtained from *h*MAOs inhibition studies, these results indicate that compound **31** can act as a multitarget agent able to prevent dopamine depletion and iron(III)-induced damage.

https://doi.org/10.1021/acs.jmedchem.1c00510
J. Med. Chem. 2021, 64, 11169−11182

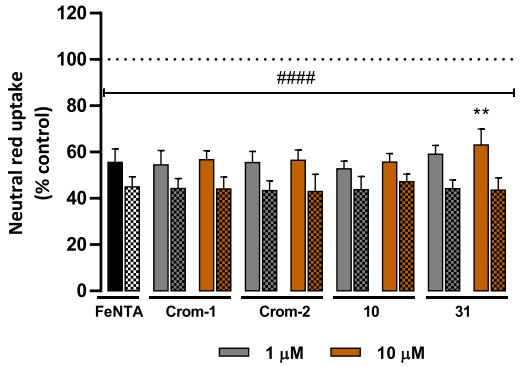

Figure 8. Evaluation of the protective effect of i-*h*MAO-B in differentiated SH-SY5Y cells against iron(III) (1000 and 1500 μM). The dashed line is the control data obtained from nontreated cells, while solid and squared bars are related with the data from cells exposed to iron(III) at 1000 and 1500 μM, respectively. The data are expressed as the means of three independent experiments together with the standard deviation (mean ± SD). Statistical comparisons were made using two-way ANOVA. In all cases, p values lower than 0.05 were considered significant ($^{\#\#\#\#}p < 0.0001$ vs the control data; $^{**}p < 0.01$ vs iron(III) values).

CONCLUSIONS

A new library of benzopyran-based compounds was synthesized, and relevant SAR and STR data were obtained. In general, the derivatives bearing chloro substituents at the exocyclic ring presented lower *h*MAO-B IC_{50} values than the 3,4-dimethyl counterparts, while compounds bearing 3,4-dimethoxy groups lacked or exhibited reduced inhibitory activity toward *h*MAO-B. These observations reinforce the data obtained so far in our previous works. Globally, our data showed for the first time the importance of the ring rigidity for *h*MAO-B inhibition and that the presence of a double bound and a carbonyl group at positions C2 or C4 of the heterocyclic ring improves *h*MAO-B inhibitory activity. We also demonstrated for the first time that while the O to N isosteric replacement abolished *h*MAO-B inhibitory activity, the O to S replacement in the chromone moiety preserved the *h*MAO-B inhibition profile of compounds. All the studies performed so far reinforce the superiority of the chemical features of the previously reported i-*h*MAO-Bs *N*-(3′,4′-dimethyl phenyl)-4-oxo-4*H*-chromene-3-carboxamide (**Crom-1**, Figure 1) and *N*-(3′-chlorophenyl)-4-oxo-4*H*-chromene-3-carboxamide (**Crom-2**, Figure 1). However, for the first time, relevant data related with thiochromones emerged. They were identified as potent and selective i-*h*MAO-Bs, with IC_{50} values within the low nM range. All the conclusions were supported by *in silico* studies that provided a rationale for the interactions of the active compounds toward *h*MAO-B and *h*MAO-A, which are consistent with the observations from the outputs of the *in vitro* biological assays.

Cytotoxicity studies showed that chromenes are safer than the related carbonyl-containing benzopyran compounds (coumarins and chromones) and that thiochromones **30** and **31** with a carbonyl group at C4 did not display remarkable cytotoxicity effects. Of particular note is *N*-(3-chlorophenyl)-4*H*-thiochromone-3-carboxamide (**31**), which exhibited potent and selective *h*MAO-B inhibition with an IC_{50} value within the low nanomolar range (*h*MAO-B IC_{50} = 1.52 ± 0.15 nM). The selected i-*h*MAO-B did not significantly affect P-gp transport activity at 10 μM. The preliminary preclinical *in vitro* ADME-toxicity studies (cytotoxicity in HUVEC, HEK-293, and MCF-7 cell lines) and cardiotoxicity (*h*ERG inhibition) indicated that compound **31** has no obvious ADME-toxicity liability.

From the gathered data, *N*-(3-chlorophenyl)-4*H*-thiochromone-3-carboxamide **31** stands out as the best potent and selective "tight binding" i-*h*MAO-B, showing a safe cytotoxicity profile in SH-SY5Y, Caco-2, HUVEC, HEK-293, and MCF-7 cells. Furthermore, compound **31** did not significantly affect P-gp activity and protected differentiated neuroblastoma cells against iron(III)-induced cell death. As such, compound **31** is a valid candidate for *in vivo* pharmacological studies.

EXPERIMENTAL SECTION

Chemistry. Details on reagents, materials, and apparatuses are provided in the SI.

Synthesis. *Synthesis of 2-Oxo-2H-chromene-2-carboxylic Acid (**13**).* Salicylaldehyde (**11**) (16.37 mmol), diethyl malonate (16.37 mmol), and catalytic amounts of piperidine (0.5 mL) were refluxed in ethanol (163.7 mL) overnight. After cooling to rt, the suspension was filtered off, and ethyl-coumarin-3-caboxylate (**12**) was obtained without further purification. **12** was refluxed in a 150 mL ethanolic solution of 0.5% NaOH (*m*/*v*) for 1 h. Then, the reaction mixture was acidified with 12 M HCl. The solid formed was isolated by filtration under reduced pressure and washed with H_2O to provide 2-oxo-2*H*-chromene-2-carboxylic acid (**13**). Yield = 61%. ^{1}H NMR (400 MHz, DMSO) δ (ppm): 7.36 (1H, d, J = 7.7 Hz, H5), 7.10 (1H, s, H4), 6.98 (1H, dd, J = 7.3, 6.9 Hz, H7), 6.71 (1H, d, J = 8.1 Hz, H8), 6.64 (1H, dd, J = 7.8, 6.8 Hz, H6).

*Synthesis of 1-Methyl-2-oxo-1,2-dihydroquinoline-3-carboxylic Acid (**19**).* To a solution of 2-oxo-1,2-dihydroquinoline-3-carboxylic acid (**18**) (4.56 mmol) in DMF (10 mL), K_2CO_3 (6.84 mmol) was added, and the reaction mixture was stirred at rt in an argon atmosphere for 20 min. Then, CH_3–I (9.12 mmol) was added dropwise, and the mixture was stirred at 60 °C for 1 h. Upon completion, water (15 mL) was added, and the mixture was extracted with DCM (3 × 15 mL). The organic layers were combined, dried over anhydrous Na_2SO_4, filtered, and concentrated under reduced pressure. The crude product was recrystallized from DCM/ethyl ether. Yield = 70%. ^{1}H NMR (400 MHz, DMSO) δ (ppm): 14.67 (1H, s, COOH), 8.97 (1H, s, H4), 8.11 (1H, dd, J = 7.9, 1.5 Hz, H8), 7.89 (1H, ddd, J = 8.6, 7.1, 1.5 Hz, H7) 7.78 (1H, dd, J = 8.6, 1.5 Hz, H5), 7.49 (1H, ddd, J = 7.9, 7.1, 1.2 Hz, H6), 3.80 (3H, s, NCH_3).

*Synthesis of Ethyl-3-(dimethylamino)-2-(2-fluorobenzoyl)-acrylate (**27**).* *N*,*N*-Dimethylformamide dimethyl acetal (5.94 mmol) was added to a solution of ethyl-(2-fluorobenzoyl)acetate (**26**) (2.73 mmol) in dry toluene (13 mL). The reaction mixture was stirred at 115 °C for 1 h. Then, the mixture was concentrated under reduced pressure. Purification by flash column chromatography (DCM/ethyl acetate 1:1) yielded compound **27**. Yield = 90%. ^{1}H NMR (400 MHz, $CDCl_3$) δ (ppm): 7.76 (1H, s, CH), 7.59 (1H, ddd, J = 7.5, 7.5, 1.8 Hz, H5), 7.38 (1H, dddd, J = 8.2, 7.1, 5.1, 1.9 Hz, H6), 7.16 (1H, ddd, J = 7.5, 7.5, 1.0 Hz, H4), 7.01 (1H, ddd, J = 10.4, 8.2, 1.1 Hz, H3), 3.96 (2H, q, J = 7.1 Hz, CH_2), 3.39–2.80 (6H, m, CH_3NCH_3), 0.89 (3H, t, J = 7.1 Hz, CH_3).

*Synthesis of Ethyl 4-Oxo-4H-thiochromene-3-carboxylate (**28**).* Hydrogen sulfide (H_2S) was bubbled into a solution of ethyl-3-(dimethylamino)-2-(2-fluorobenzoyl)acrylate (**27**) (3.20 mmol) in THF (60 mL) at −30 °C for 4 h. The mixture was concentrated, and the crude product was purified by chromatography to afford compound **28**. Yield = 80%. ^{1}H NMR (400 MHz, DMSO) δ (ppm): 7.70 (1H, s, H2), 7.50–7.38 (2H, m, H5, H7), 7.23–7.19 (1H, m, H8), 7.16 (ddd, J = 10.7, 8.3, 1.1 Hz, H6), 3.84 (2H, q, J = 7.1 Hz, CH_2), 0.84 (3H, t, J = 7.1 Hz, CH_3).

*Synthesis of 4-Oxo-4H-thiochromene-3-carboxylic Acid (**29**).* A mixture of ethyl 4-oxo-4*H*-thiochromene-3-carboxylate (**28**) (2.13 mmol), acetic acid (54 mL), H_2O (15 mL), and HCl (1.5 mL) was heated on a steam bath for 4 h. The reaction mixture was concentrated under reduced pressure, and the product obtained was recrystallized from DCM/petroleum ether to give the compound **29**. Yield = 40%. ^{1}H NMR (400 MHz, $CDCl_3$) δ (ppm): 15.12 (1H, s, COOH), 8.07 (1H, s,

https://doi.org/10.1021/acs.jmedchem.1c00510
J. Med. Chem. 2021, 64, 11169−11182

H2), 8.25 (1H, ddd, J = 8.5, 1.3, 0.6 Hz, H5), 7.90 (1H, ddd, J = 8.5, 6.9, 1.3 Hz, H7), 7.70 (1H, ddd, J = 8.5, 1.3, 0.6 Hz, H8), 7.62 (1H, ddd, J = 8.5, 6.9, 1.3 Hz, H6).

General Procedure A: Synthesis of Chromane (2−5), Chromene (7−10), Coumarin (14−17), and Thiochromone (30 and 31) Derivatives. A solution of the appropriate heterocyclic carboxylic acid (chromane-3-carboxylic acid (**1**), chromene-3-carboxylic acid (**6**), 2-oxo-2*H*-chromene-3-carboxylic acid (**13**), or thiochromone-3-carboxylic acid (**29**)) (2.8 mmol) and $POCl_3$ (4.2 mmol) in DMF (4.2 mL) was stirred at rt for 15 min. Then, the appropriate amine (5.61 mmol) was added, and the mixture was stirred at rt overnight. Following the addition of DCM (50 mL), the mixture was extracted with H_2O (3 × 15 mL), 1 M HCl (3 × 15 mL) and saturated aqueous solution of $NaHCO_3$ (3 × 5 mL). The organic layers were combined, dried over anhydrous Na_2SO_4, filtered, and concentrated under reduced pressure. The crude product was purified by recrystallization.

*N-(3,4-Dimethylphenyl)chromane-3-carboxamide (**2**).* Compound **2** was recrystallized from DCM/ethyl ether. Yield = 56%. ^{1}H NMR (400 MHz, $CDCl_3$) δ (ppm): 7.53 (1H, s, CONH), 7.28 (1H, d, J = 2.3 Hz, H2′), 7.19 (1H, dd, J = 8.1, 2.4 Hz, H6′), 7.15−7.10 (1H, m, H6), 7.08 (1H, dd, J = 7.7, 1.3 Hz, H5), 7.05 (1H, d, J = 8.1 Hz, H5′), 6.90 (1H, dd, J = 7.4, 1.3 Hz, H8), 6.87−6.84 (1H, m, H7), 4.48−4.17 (2H, m, H2), 3.22 (1H, dd, J = 16.4, 9.4 Hz, H3), 3.04−2.85 (2H, m, H4), 2.22 (3H, s, 3′CH_3), 2.21 (3H, s, 4′CH_3). ^{13}C NMR (100 MHz, $CDCl_3$) δ (ppm): 170.2, 153.8, 137.3, 135.1, 133.1, 130.0, 129.9, 127.7, 121.5, 121.0, 120.4, 117.6, 116.8, 67.2, 40.8, 28.4, 19.8, 19.1. EI/MS m/z (%): 55 (12), 77 (24), 79 (12) 105 (22), 106 (16), 120 (16), 121 (92), 131 (13), 133 (13), 237 (12), 281 (M^+, 100), 282 (M^+ + 1, 19).

*N-(3-Chlorophenyl)chromane-3-carboxamide (**3**).* Compound **3** was recrystallized from DCM/ethyl ether. Yield = 54%. ^{1}H NMR (400 MHz, DMSO) δ (ppm): 10.37 (1H, s, CONH), 7.84 (1H, dd, J = 2.1, 2.1 Hz, H2′), 7.48 (1H, ddd, J = 8.2, 2.1, 1.0 Hz, H6′), 7.35 (1H, dd, J = 8.0, 8.0 Hz, H5′), 7.17−7.06 (3, m, H5, H6, H4′), 6.86 (1H, ddd, J = 7.4, 7.4, 1.2 Hz, H7), 6.79 (1H, dd, J = 8.2, 1.2 Hz, H8), 4.49−3.96 (2H, m, H2), 3.11−2.91 (3H, m, H3, H4). ^{13}C NMR (100 MHz, DMSO) δ (ppm): 170.6, 153.6, 140.3, 133.0, 130.4, 129.7, 127.1, 123.0, 121.0, 120.3, 118.6, 117.5, 116.1, 66.8, 39.2, 27.3. EI/MS m/z (%): 51 (19), 55 (39), 77 (44), 79 (22), 103 (23), 129 (26), 131 (59), 132 (60), 133 (74), 134 (18), 243 (16), 287 (M^+, 100), 288 (M^+ + 1, 18), 289 (M^+ + 2, 33).

*N-(3,4-Dimethoxyphenyl)chromane-3-carboxamide (**4**).* Compound **4** was recrystallized from ethyl acetate/*n*-hexane. Yield = 45%. ^{1}H NMR (400 MHz, DMSO) δ (ppm): 10.04 (1H, s, CONH), 7.34 (1H, d, J = 2.4 Hz, H2′), 7.14 (1H, dd, J = 7.6, 1.6 Hz, H6′), 7.14−7.04 (2H, m, H5, H6), 6.89 (1H, d, J = 8.7 Hz, H5′), 6.86 (1H, ddd, J = 7.40, 7.39, 1.26 Hz, H7), 6.78 (1H, dd, J = 8.1, 1.2 Hz, H8), 4.50−3.93 (2H, m, H2), 3.73 (3H, s, 3′OCH_3), 3.72 (3H, s, 4′OCH_3), 3.07−2.90 (3H, m, H4, H3). ^{13}C NMR (100 MHz, DMSO) δ (ppm): 170.3, 154.2, 149.0, 145.4, 133.1, 130.3, 127.6, 121.7, 120.8, 116.6, 112.5, 111.6, 104.9, 67.5, 56.2, 55.8, 39.6, 28.0. EI/MS m/z (%): 77 (11), 105 (17), 133 (14), 138 (52), 151 (11), 153 (57), 313 (M^+, 100), 314 (21).

*N-(3,4-Dichlorophenyl)chromane-3-carboxamide (**5**).* Compound **5** was recrystallized from DCM/ethyl ether. Yield = 36%. ^{1}H NMR (400 MHz, DMSO) δ (ppm): 10.47 (1H, s, CONH), 8.01 (1H, d, J = 2.4 Hz, H2′), 7.58 (1H, d, J = 8.8 Hz, H5′), 7.51 (1H, dd, J = 8.8, 2.4 Hz, H6′), 7.14 (1H, dd, J = 7.6, 1.6 Hz, H5), 7.09 (1H, ddd, J = 8.1, 7.3, 1.7 Hz, H6), 6.86 (1H, ddd, J = 7.4, 7.4, 1.2 Hz, H7), 6.79 (1H, dd, J = 8.1, 1.3 Hz, H8), 4.48−3.98 (2H, m, H2), 3.06−2.93 (3H, m, H3, H4). ^{13}C NMR (100 MHz, DMSO) δ (ppm): 170.7, 153.6, 138.9, 130.9, 130.6, 129.7, 127.1, 124.7, 121.0, 120.3 (2 × ^{13}C), 119.2, 116.1, 66.7, 39.3, 27.2. EI/MS m/z (%): 77 (54), 78 (18), 79 (27), 103 (24), 105 (83), 131 (49), 132 (51), 133 (98), 134 (18), 160 (20), 161 (88), 163 (48), 277 (18), 321 (100), 322 (M^+, 18), 323 (M^+ + 1, 63), 324 (M^+ + 2, 12).

*N-(3,4-Dimethylphenyl)-2H-chromene-3-carboxamide (**7**).* Compound **7** was recrystallized from DCM/ethyl ether. Yield = 43%. ^{1}H NMR (400 MHz, CDCl3) δ (ppm): 7.54 (1H, s, CONH), 7.35 (1H, d, J = 2.3 Hz, H2′), 7.27 (1H, dd, J = 8.0, 2.3 Hz, H5), 7.22 (1H, ddd, J = 8.1, 7.4, 1.7 Hz, H7), 7.13−7.05 (2H, m, H6′, H8), 7.05 (1H, s, H4), 6.92 (1H, ddd, J = 7.4, 7.4, 1.1 Hz, H6), 6.86 (1H, d, J = 8.1 Hz, H5′), 5.06 (2H, d, J = 1.3 Hz, H2), 2.24 (3H, s, 3′CH3), 2.22 (3H, s, 4′CH3). ^{13}C NMR (100 MHz, CDCl3) δ (ppm): 163.2, 154.9, 137.4, 135.1, 133.1, 131.5, 130.1, 128.4, 127.4, 127.2, 121.8, 121.6, 120.8, 117.7, 116.2, 64.9, 19.9, 19.2. EI/MS m/z (%): 77 (23), 115 (28), 131 (22), 159 (100), 278 (15), 279 (M^+, 90), 280 (M^+ + 1, 18).

*N-(3-Chlorophenyl)-2H-chromene-3-carboxamide (**8**).* Compound **8** was recrystallized from ethyl acetate/*n*-hexane. Yield = 28%. ^{1}H NMR (400 MHz, $CDCl_3$) δ (ppm): 7.69 (1H, dd, J = 2.1, 2.1 Hz, H2′), 7.59 (1H, s, CONH), 7.42 (1H, ddd, J = 8.2, 2.1, 1.0 Hz, H6′), 7.28 (1H, ddd, J = 8.2, 1.5, 1.5 Hz, H4′), 7.24 (1H, dd, J = 6.05, 1.78, H5), 7.14−7.10 (2H, m, H7, H5′), 7.08 (1H, s, H4), 6.94 (1H, ddd, J = 7.5, 7.5, 1.1 Hz, H6), 6.88 (1H, d, J = 8.1 Hz, H8), 5.06 (2H, d, J = 1.3 Hz, H2). ^{13}C NMR (100 MHz, $CDCl_3$) δ (ppm): 163.2, 155.0, 138.6, 134.8, 131.9, 130.1, 128.5, 127.9, 126.8, 124.7, 121.9, 120.6, 120.2, 118.0, 116.3, 64.7. EI/MS m/z (%): 51 (10), 77 (22), 115 (26), 131 (17), 159 (100), 160 (11), 285 (M^+, 45), 286 (M^+ + 1, 9), 287 (M^+ + 2, 15).

*N-(3,4-Dimethoxyphenyl)-2H-chromene-3-carboxamide (**9**).* Compound **9** was recrystallized from ethyl acetate/*n*-hexane. Yield = 25%. ^{1}H NMR (400 MHz, DMSO) δ (ppm): 9.91 (1H, s, CONH), 7.44 (1H, s, H4), 7.39 (1H, d, J = 2.4 Hz, H2′), 7.31−7.24 (2H, m, H5, H7), 7.25 (1H, dd, J = 8.8, 2.1 Hz, H6′), 6.99 (1H, ddd, J = 7.4, 7.4, 1.1 Hz, H6), 6.92 (1H, d, J = 8.8 Hz, H5′), 6.88 (1H, dd, J = 7.8, 1.0 Hz, H8), 4.98 (2H, d, J = 1.4 Hz, H2), 3.74 (3H, s, 3′OCH_3), 3.73 (3H, s, 4′OCH_3). ^{13}C NMR (100 MHz, DMSO) δ (ppm): 163.4, 154.7, 148.9, 145.6, 132.8, 131.6, 129.0, 127.9, 127.5, 122.4, 121.7, 116.2, 112.6, 112.4, 105.7, 64.9, 56.2, 55.8. EI/MS m/z (%): 77 (17), 115 (33), 131 (20), 159 (100), 292 (13), 311 (M^+, 80), 312 (15).

*N-(3,4-Dichlorophenyl)-2H-chromene-3-carboxamide (**10**).* Compound **10** was recrystallized from DCM/ethyl ether. Yield = 21%. ^{1}H NMR (400 MHz, DMSO) δ (ppm): 10.29 (1H, s, CONH), 8.07 (1H, d, J = 2.4 Hz, H2′), 7.68 (1H, dd, J = 8.8, 2.4 Hz, H6′), 7.60 (1H, d, J = 8.8 Hz, H5′), 7.50 (1H, s, H4), 7.32−7.25 (2H, m, H7, H5), 7.00 (1H, ddd, J = 7.4, 7.4, 1.1 Hz, H6), 6.89 (1H, dd, J = 7.4, 1.1 Hz, H8), 4.98 (2H, d, J = 1.3 Hz, H2). ^{13}C NMR (100 MHz, DMSO) δ (ppm): 164.1, 154.8, 139.5, 132.0, 131.3, 131.1, 129.2, 129.1, 126.8, 125.5, 122.4, 121.6, 121.4, 120.4, 116.3, 64.7. EI/MS m/z (%): 77 (24), 102 (9), 103 (10), 115 (34), 131 (17), 159 (100), 160 (11), 319 (16), 320 (M^+, 3), 321 (M^+ + 1, 10), 322 (M^+ + 2, 2).

*N-(3,4-Dimethylphenyl)-2-oxo-2H-chromene-3-carboxamide (**14**).* Compound **14** was recrystallized from ethyl acetate/*n*-hexane. Yield = 45%. ^{1}H NMR (400 MHz, DMSO) δ (ppm): 10.55 (1H, s, CONH), 8.91 (1H, s, H4), 8.01 (1H, dd, J = 7.7, 1.6 Hz, H5), 7.78 (1H, ddd, J = 8.8, 7.4, 1.6 Hz, H7), 7.55 (1H, dd, J = 8.4, 2.2 Hz, H6′), 7.52−7.47 (2H, m, H2′, H8), 7.46−7.44 (1H, m, H6), 7.13 (1H, d, J = 8.1 Hz, H5′), 2.23 (3H, s, 3′CH_3), 2.20 (3H, s, 4′CH_3). ^{13}C NMR (100 MHz, DMSO) δ (ppm): 160.5, 159.4, 153.8, 147.2, 136.7, 135.6, 134.1, 132.1, 130.2, 129.8, 125.2, 120.9, 119.8, 118.4, 117.2, 116.1, 19.4, 18.7. EI/MS m/z (%): 89 (13), 101 (16), 173 (100), 174 (11), 264 (10), 265 (14), 293 (M^+, 79), 294 (M^+ + 1, 16).

*N-(3-Chlorophenyl)-2-oxo-2H-chromene-3-carboxamide (**15**).* Compound **15** was recrystallized from ethyl acetate/*n*-hexane. Yield = 42%. ^{1}H NMR (400 MHz, DMSO) δ (ppm): 10.76 (1H, s, CONH), 8.91 (1H, s, H4), 8.02 (1H, dd, J = 7.8, 1.6 Hz, H5), 7.98 (1H, dd, J = 2.0, 2.0 Hz, H2′), 7.79 (1H, ddd, J = 8.9, 7.4, 1.6 Hz, H7), 7.60−7.54 (2H, m, H4′, H6′), 7.48 (1H, ddd, J = 7.5, 7,52, 1.1 Hz, H6), 7.42 (1H, dd, J = 8.1, 8.0 Hz, H5′), 7.22 (1H, ddd, J = 7.9, 2.1, 0.9 Hz, H8). ^{13}C NMR (100 MHz, DMSO) δ (ppm): 160.3, 160.0, 153.8, 147.4, 139.3, 134.3, 133.2, 130.6, 130.2, 125.2, 124.0, 119.8, 119.4, 118.4, 118.3, 116.2. EI/MS m/z (%): 63 (8), 89 (14), 101 (14), 173 (100), 174 (11), 299 (M^+, 26), 301 (M^+ + 2, 9).

*N-(3,4-Dimethoxyphenyl)-2-oxo-2H-chromene-3-carboxamide (**16**).* Compound **16** was recrystallized from ethyl acetate/*n*-hexane. Yield = 53%. ^{1}H NMR (400 MHz, DMSO) δ (ppm): 10.53 (1H, s, CONH), 8.91 (1H, s, H4), 8.01 (1H, dd, J = 7.8, 1.6 Hz, H5), 7.78 (1H, ddd, J = 8.4, 7.3, 1.6 Hz, H7), 7.56 (1H, d, J = 8.4 Hz, H5′), 7.48 (1H, ddd, J = 7.7, 7.7, 1.1 Hz, H6), 7.39 (1H, d, J = 2.4 Hz, H2′), 7.29 (1H, dd, J = 8.4, 2.4 Hz, H6′), 6.96 (1H, dd, J = 7.8, 1.6, Hz, H8), 3.78 (3H, s, 3′OCH_3), 3.75 (3H, s, 4′OCH_3). ^{13}C NMR (100 MHz, DMSO) δ

https://doi.org/10.1021/acs.jmedchem.1c00510
J. Med. Chem. 2021, 64, 11169−11182

(ppm): 160.4, 159.3, 153.8, 148.6, 147.2, 145.5, 134.1, 131.3, 130.2, 125.2, 119.8, 118.4, 116.1, 112.0, 111.9, 104.9, 55.6, 55.4. EI/MS *m/z* (%): 89 (10), 101 (11), 173 (100), 174 (11), 310 (24), 325 (M^+, 82), 326 (17).

*N-(3,4-Dichlorophenyl)-2-oxo-2H-chromene-3-carboxamide (**17**).* Compound **17** was recrystallized from ethyl acetate/*n*-hexane. Yield = 25%. ^{1}H NMR (400 MHz, MeOD) δ (ppm): 9.20 (1H, s, H4), 8.22 (1H, d, *J* = 2.4 Hz, H2′), 7.99 (1H, dd, *J* = 7.7, 1.6 Hz, H5), 7.95 (1H, ddd, *J* = 8.8, 7.3, 1.6 Hz, H7), 7.72 (1H, dd, *J* = 8.7, 2.5 Hz, H6′), 7.68−7.67 (1H, m, H5′), 7.66−7.64 (2H, m, H8, H6). ^{13}C NMR and DEPT 135 data (*). MS/EI *m/z* (%): 63 (12), 89 (22), 101 (21), 173 (100), 174 (11), 333 (15), 334 (M^+, 3), 335 (M^+ + 1, 10), 336 (M^+ + 2, 1).

*N-(3,4-Dimethylphenyl)-4-oxo-4H-thiochromene-3-carboxamide (**30**).* Compound **30** was recrystallized from DCM/ethyl ether. Yield = 25%. ^{1}H NMR (400 MHz, $CDCl_3$) δ (ppm): 11.28 (1H, s, CONH), 9.07 (1H, s, H2), 8.34 (1H, dd, *J* = 8.0, 1.7 Hz, H5), 7.79 (1H, ddd, *J* = 8.7, 7.1, 1.7 Hz, H7), 7.59 (1H, dd, *J* = 8.6, 1.1 Hz, H8), 7.56−7.53 (1H, m, H6), 7.52 (1H, d, *J* = 1.2 Hz, H2′), 7.48 (1H, dd, *J* = 8.1, 2.4 Hz, H6′), 7.12 (1H, d, *J* = 8.1 Hz, H5′), 2.28 (3H, s, 3′CH_3), 2.24 (3H, s, 4′CH_3). ^{13}C NMR (100 MHz, $CDCl_3$) δ (ppm): 177.4, 162.7, 160.5, 156.2, 137.2, 135.7, 134.8, 132.8, 130.0, 126.4, 126.2, 124.1, 121.8, 118.5, 118.0, 116.1, 19.9, 19.2. EI/MS *m/z* (%): 53 (15), 77 (9), 121 (63), 122 (9), 145 (9), 173 (100), 174 (11), 293 (91), 294 (18).

*N-(3-Chlorophenyl)-4-oxo-4H-thiochromene-3-carboxamide (**31**).* Compound **31** was recrystallized from DCM/ethyl ether. Yield = 20%. ^{1}H NMR (400 MHz, $CDCl_3$) δ (ppm): 11.49 (1H, s, CONH), 9.07 (1H, s, H2), 8.34 (1H, ddd, *J* = 6.4, 1.3, 0.4 Hz, H5), 7.90 (1H, dd, *J* = 2.04, 2.04 Hz, H2′), 7.81 (1H, ddd, *J* = 8.7, 7.1, 1.7 Hz, H7), 7.61 (1H, dd, *J* = 7.8, 1.8 Hz, H8), 7.58−7.53 (2H, m, H6, H6′), 7.29 (1H, dd, *J* = 8.13, 8.13 Hz, H5′), 7.12 (1H, ddd, *J* = 7.9, 2.0, 1.0 Hz, H4′). ^{13}C NMR (100 MHz, $CDCl_3$) δ (ppm): 177.4, 163.0, 160.9 (CONH), 156.2 (C8a), 139.1, 135.0, 134.6, 129.9, 126.6, 126.3, 124.5, 124.0, 120.6, 118.6, 118.5, 115.7. EI/MS *m/z* (%): 53 (17), 89 (9), 120 (4), 121 (58), 123 (7), 145 (3), 172 (3), 173 (100), 174 (11), 299 (51), 300 (9), 301 (17), 315 (M^+, 2).

General Procedure B: Synthesis of 2-Oxo-1,2-dihydroquinoline-3-carboxamide (20−22) and *N*-1-Methyl-2-oxo-1,2-dihydroquinoline-3-carboxamide (23−25) Derivatives. A solution of the appropriate heterocyclic carboxylic acid (2-oxo-1,2-dihydroquinoline-3-carboxylic acid (**18**) or *N*-1-methyl-2-oxo-1,2-dihydroquinoline-3-carboxylic acid (**19**)) (1.05 mmol), TBTU (1.05 mmol), and DIPEA (2.1 mmol) in DMF (10 mL) was stirred at rt for 15 min. Then, the appropriate amine (1.26 mmol) was added, and the mixture was stirred at room temperature overnight. Then, DCM (50 mL) was added, and the mixture was extracted with H_2O (3 × 5 mL), 1 M HCl (3 × 5 mL), and saturated aqueous solution of $NaHCO_3$ (3 × 5 mL). The organic layers were combined, washed with aqueous solution of 10% NaOH (*m/v*), dried over anhydrous Na_2SO_4, filtered, and concentrated. The crude product was purified by recrystallization.

*N-(3,4-Dimethylphenyl)-2-oxo-1,2-dihydroquinoline-3-carboxamide (**20**).* Compound **20** recrystallized from MeOH/*n*-hexane. Yield = 40%. ^{1}H NMR (400 MHz, DMSO) δ (ppm): 12.63 (1H, s, CONH), 12.01 (1H, s, NH), 8.96 (1H, s, H4), 8.00 (1H, dd, *J* = 6.7, 1.1 Hz, H8), 7.70 (1H, ddd, *J* = 7.1, 6.0, 1.5 Hz, H7), 7.52 (1H, dd, *J* = 8.3, 2.1 Hz, H5), 7.48 (1H, dd, *J* = 8.2, 2.2 Hz, H6′), 7.45 (1H, d, *J* = 2.2 Hz, H2′), 7.34 (1H, ddd, *J* = 7.0, 6.2, 1.5 Hz, H6), 7.13 (1H, d, *J* = 8.1 Hz, H5′), 2.24 (3H, s, 3′CH_3), 2.20 (3H, s, 4′CH_3). ^{13}C NMR (100 MHz, DMSO) δ (ppm): 162.1, 160.6, 144.2, 141.00, 139.4, 136.7, 135.9, 132.9 (2 × ^{13}C), 131.7, 129.8, 127.5, 123.0, 120.8, 117.1, 115.4, 19.4, 18.7. EI/MS *m/z* (%): 57 (15), 89 (30), 116 (48), 121 (87), 128 (12), 172 (92), 173 (11), 292 (M^+, 100), 293 (22).

*N-(3-Chlorophenyl)-2-oxo-1,2-dihydroquinoline-3-carboxamide (**21**).* Compound **21** was recrystallized from ethyl acetate/*n*-hexane. Yield = 50%. ^{1}H NMR (400 MHz, DMSO) δ (ppm): 12.68 (1H, s, CONH), 12.27 (1H, s, NH), 8.98 (1H, s, H4), 8.03−8.00 (2H, m, H8, H2′), 7.72 (1H, ddd, *J* = 8.5, 7.1, 1.4 Hz, H7), 7.54 (1H, ddd, *J* = 8.2, 2.1, 1.0 Hz, H6′), 7.49 (1H, dd, *J* = 8.3, 1.3 Hz, H5), 7.41 (1H, dd, *J* = 8.0, 8.0 Hz, H5′), 7.35 (1H, ddd, *J* = 8.1, 7.1, 1.1 Hz, H6), 7.20 (1H, ddd, *J* = 8.0, 2.2, 1.0 Hz, H4′). ^{13}C NMR (100 MHz, DMSO) δ (ppm): 162.6, 161.9, 145.3, 140.1, 140.0, 133.8, 133.7, 131.2, 130.5, 124.2, 123.6, 121.5, 119.8, 119.2, 118.8, 116.0. EI/MS *m/z* (%): 63 (8), 89 (23), 116 (46), 117 (8), 128 (11), 144 (3), 172 (100), 173 (11), 298 (M^+, 33), 299 (M^+ + 1, 7), 300 (M^+ + 2, 12).

*N-(3,4-Dichlorophenyl)-2-oxo-1,2-dihydroquinoline-3-carboxamide (**22**).* Compound **22** was recrystallized from MeOH/ethyl ether. Yield = 40%. ^{1}H NMR (400, MHz, DMSO) δ (ppm): 12.60 (1H, s, CONH), 12.05 (1H, s, NH), 8.45 (1H, s, H4), 7.90 (1H, d, *J* = 2.4 Hz, H2′), 7.83 (1H, dd, *J* = 7.5, 1.7 Hz, H5), 7.75 (1H, dd, *J* = 7.1, 2.4 Hz, H6′), 7.60 (1H, d, *J* = 7.1 Hz, H5′), 7.50 (1H, dd, *J* = 7.5, 1.5 Hz, H8), 7.30−7.26 (2H, m, H7, H6). ^{13}C NMR and DEPT 135 data (*). EI/MS *m/z* (%): 89 (23), 116 (40), 128 (10), 172 (100), 173 (11), 332 (29), 333 (M^+, 6), 334 (M^+ + 1, 19), 335 (M^+ + 2, 3), 337 (M^+ + 4, 6).

*N-(3,4-Dimethylphenyl)-1-methyl-2-oxo-1,2-dihydroquinoline-3-carboxamide (**23**).* Compound **23** was recrystallized from ethyl acetate/*n*-hexane. Yield = 35%. ^{1}H NMR (400 MHz, DMSO) δ (ppm): 12.00 (1H, s, CONH) 8.95 (1H, s, H4), 8.07 (1H, dd, *J* = 7.8, 1.5 Hz, H8), 7.82 (1H, ddd, *J* = 8.6, 7.1, 1.5 Hz, H7), 7.71 (1H, dd, *J* = 8.5 Hz, 1.5 Hz, H5), 7.53 (1H, dd, *J* = 8.1, 2.0 Hz, H6′), 7.46 (1H, d, *J* = 2.0 Hz, H2′), 7.43 (1H, ddd, *J* = 7.9, 7.1, 1.2 Hz, H6), 7.13 (1H, d, *J* = 8.1 Hz, H5′), 3.79 (3H, s, NCH_3), 2.24 (3H, s, 3′CH_3), 2.20 (3H, s, 4′CH_3). ^{13}C NMR (100 MHz, DMSO) δ (ppm): 161.4, 160.5, 143.4, 140.2, 136.7, 135.9, 133.3, 131.8, 130.8, 129.8, 123.1, 120.9, 120.8, 119.2, 117.1, 115.3, 29.9, 19.4, 18.7. EI/MS *m/z* (%): 89 (19), 91 (5), 186 (100), 277 (11), 278 (10), 306 (M^+, 99), 307 (M^+ + 1, 19).

*N-(3-Chlorophenyl)-1-methyl-2-oxo-1,2-dihydroquinoline-3-carboxamide (**24**).* Compound **24** was recrystallized from MeOH/*n*-hexane. Yield = 22%. ^{1}H NMR (400 MHz, DMSO) δ (ppm): 12.22 (1H, s, CONH), 8.97 (1H, s, H4), 8.07 (1H, dd, *J* = 7.9, 1.3 Hz, H8), 8.03 (1H, dd, *J* = 2.0, 2.0 Hz, H2′), 7.83 (1H, ddd, *J* = 8.6, 7.1, 1.5 Hz, H7), 7.72 (1H, d, *J* = 8.6 Hz, H5), 7.55 (1H, ddd, *J* = 8.1, 1.9, 1.5 Hz, H6′), 7.43 (1H, ddd, *J* = 7.5, 7.5, 1.8 Hz, H6), 7.40 (1H, d, *J* = 8.1 Hz, H5′), 7.20 (1H, ddd, *J* = 8.0, 2.0, 1.5 Hz, H4′), 3.80 (3H, s, NCH_3). ^{13}C NMR and DEPT 135 data (a). MS/EI *m/z* (%): 89 (13), 128 (3), 130 (4), 185 (3), 186 (100), 312 (M^+, 35), 313 (M^+ + 1, 6), 314 (M^+ + 2, 12).

*N-(3,4-Dichlorophenyl)-1-methyl-2-oxo-1,2-dihydroquinoline-3-carboxamide (**25**).* Compound **25** was recrystallized from MeOH/*n*-hexane. Yield = 20%. ^{1}H NMR (400 MHz, DMSO) δ (ppm): 12.14 (1H, s, CONH), 8.93 (1H, s, H4), 8.15 (1H, dd, *J* = 8.1, 2.0 Hz, H6′), 8.07 (1H, dd, *J* = 7.8, 1.5 Hz, H8), 7.82 (1H, dd, *J* = 7.9, 7.9 Hz, H7), 7.70 (1H, dd, *J* = 8.5 Hz, 1.5 Hz H5), 7.61 (1H, d, *J* = 6.08 Hz, H5′), 7.50−7.43 (2H, m, H6, H2′), 3.80 (3H, s, NCH_3). ^{13}C NMR and DEPT 135 data (*). EI/MS *m/z* (%): 55 (19), 57 (20), 89 (22), 128 (9), 186 (100), 187 (14), 346 (36), 348 (M^+ + 1, 21).

(*) ^{13}C NMR was not acquired due to solubility constraints.

The purity of the final products (>98%) was verified by high-performance liquid chromatography (HPLC) equipped with a DAD detector (Figures S9−S26).

Pharmacology. The details about monoamine oxidase inhibitory assays, cytotoxicity studies, and computational simulations are provided in the SI.

■ ASSOCIATED CONTENT

Supporting Information

The Supporting Information is available free of charge at https://pubs.acs.org/doi/10.1021/acs.jmedchem.1c00510.

Molecular formula strings (CSV)

PDB files of homology (ZIP)

Enzymatic assays, *in vitro* toxicology, computational studies, supplementary tables, and figures (PDF)

■ AUTHOR INFORMATION

Corresponding Authors

Alexandra Gaspar − *CIQUP/Department of Chemistry and Biochemistry, Faculty of Sciences, University of Porto, Porto 4169-007, Portugal*; Email: alexandra.gaspar@fc.up.pt

Fernanda Borges − *CIQUP/Department of Chemistry and Biochemistry, Faculty of Sciences, University of Porto, Porto 4169-007, Portugal;* orcid.org/0000-0003-1050-2402; Email: fborges@fc.up.pt

Authors

Francesco Mesiti − *Dipartimento di Scienze della Salute, Università "Magna Græcia" di Catanzaro, Campus "Salvatore Venuta", Catanzaro 88100, Italy; Net4Science srl, Academic Spinoff, Università "Magna Græcia" di Catanzaro, Campus "Salvatore Venuta", Catanzaro 88100, Italy; CIQUP/Department of Chemistry and Biochemistry, Faculty of Sciences, University of Porto, Porto 4169-007, Portugal*

Daniel Chavarria − *CIQUP/Department of Chemistry and Biochemistry, Faculty of Sciences, University of Porto, Porto 4169-007, Portugal*

Annalisa Maruca − *Dipartimento di Scienze della Salute, Università "Magna Græcia" di Catanzaro, Campus "Salvatore Venuta", Catanzaro 88100, Italy; Net4Science srl, Academic Spinoff, Università "Magna Græcia" di Catanzaro, Campus "Salvatore Venuta", Catanzaro 88100, Italy*

Roberta Rocca − *Net4Science srl, Academic Spinoff, Università "Magna Græcia" di Catanzaro, Campus "Salvatore Venuta", Catanzaro 88100, Italy; Department of Experimental and Clinical Medicine, "Magna Græcia" University of Catanzaro, Campus "S. Venuta", Catanzaro 88100, Italy;* orcid.org/0000-0002-0680-7097

Eva Gil Martins − *UCIBIO-REQUIMTE, Laboratory of Toxicology, Department of Biological Sciences, Faculty of Pharmacy, University of Porto, Porto 4050-313, Portugal*

Sandra Barreiro − *UCIBIO-REQUIMTE, Laboratory of Toxicology, Department of Biological Sciences, Faculty of Pharmacy, University of Porto, Porto 4050-313, Portugal*

Renata Silva − *UCIBIO-REQUIMTE, Laboratory of Toxicology, Department of Biological Sciences, Faculty of Pharmacy, University of Porto, Porto 4050-313, Portugal;* orcid.org/0000-0001-9962-7548

Carlos Fernandes − *CIQUP/Department of Chemistry and Biochemistry, Faculty of Sciences, University of Porto, Porto 4169-007, Portugal;* orcid.org/0000-0002-0102-0703

Sheraz Gul − *Fraunhofer Institute for Translational Medicine and Pharmacology, Hamburg 22525, Germany; Fraunhofer Cluster of Excellence for Immune-Mediated Diseases CIMD, Hamburg 22525, Germany*

Oliver Keminer − *Fraunhofer Institute for Translational Medicine and Pharmacology, Hamburg 22525, Germany; Fraunhofer Cluster of Excellence for Immune-Mediated Diseases CIMD, Hamburg 22525, Germany*

Stefano Alcaro − *Dipartimento di Scienze della Salute, Università "Magna Græcia" di Catanzaro, Campus "Salvatore Venuta", Catanzaro 88100, Italy*

Complete contact information is available at: https://pubs.acs.org/10.1021/acs.jmedchem.1c00510

Author Contributions

The manuscript was written through contributions of all authors. All authors have given approval to the final version of the manuscript.

Funding

This project was supported by the Foundation for Science and Technology (FCT) and FEDER/COMPETE (Grants UID/QUI/00081/2020 and PTDC/MED-QUI/29164/2017). This article is based upon work from COST Action CA15135.

Notes

The authors declare no competing financial interest.

■ ABBREVIATIONS

(ATP), adenosine tri-phosphate; (BBB), blood−brain barrier; (CNS), central nervous system; (Caco-2), colon adenocarcinoma cells; (TBTU), 2-(1*H*-benzotriazole-1-yl)-1,1,3,3-tetramethylaminium tetrafluoroborate; (coul), Coulomb; (DCM), dichloromethane; (Crom-2), *N*-(3′-chlorophenyl)-4-oxo-4*H*-chromene-3-carboxamide; (Crom-1), *N*-(3′,4′-dimethyl phenyl)-4-oxo-4*H*-chromene-3-carboxamide; (DIPEA), *N*,*N*-diisopropylethylamine; (DMF), dimethylformamide; (FP), fluorescence polarization; (PDB code 2Z5X), *h*MAO-A; (PDB code 6FW0), *h*MAO-B; (HBA), hydrogen bond acceptors; (MCF-7), human breast adenocarcinoma cell-line Michigan Cancer Foundation-7 cells; (HEK-293), human embryonic kidney 293 cells; (HUVEC), human umbilical vein endothelial cells; (HBD), hydrogen bond donors; (MTT), methylthiazolyldiphenyltetrazolium bromide; (MW), molecular weight; (MAO-A and MAO-B), monoamine oxidases A and B; (i-*h*MAO-B), MAO-B inhibitors; (SH-SY5Y), neuroblastoma cells; (NR), neutral red; (PD), Parkinson's disease; (RHO 123), Rhodamine 123; (RB), rotatable bonds; (SAR), structure−activity relationship; (STR), structure−toxicity relationship; (tPSA in $Å^2$), topological polar surface area; (XP G-Score), XP Glide Score; (vdW), van der Waals

■ REFERENCES

(1) Gealageas, R.; Devineau, A.; So, P. P. L.; Kim, C. M. J.; Surendradoss, J.; Buchwalder, C.; Heller, M.; Goebeler, V.; Dullaghan, E. M.; Grierson, D. S.; Putnins, E. E. Development of novel monoamine oxidase-B (MAO-B) inhibitors with reduced blood-brain barrier permeability for the potential management of noncentral nervous system (CNS) diseases. *J. Med. Chem.* **2018**, *61*, 7043−7064.

(2) Finberg, J. P.; Rabey, J. M. Inhibitors of MAO-A and MAO-B in psychiatry and neurology. *Front. Pharmacol.* **2016**, *7*, 340.

(3) Tripathi, R. K. P.; Ayyannan, S. R. Monoamine oxidase-B inhibitors as potential neurotherapeutic agents: an overview and update. *Med. Res. Rev.* **2019**, *39*, 1603−1706.

(4) Park, J. H.; Ju, Y. H.; Choi, J. W.; Song, H. J.; Jang, B. K.; Woo, J.; Chun, H.; Kim, H. J.; Shin, S. J.; Yarishkin, O.; Jo, S.; Park, M.; Yeon, S. K.; Kim, S.; Kim, J.; Nam, M. H.; Londhe, A. M.; Kim, J.; Cho, S. J.; Cho, S.; Lee, C.; Hwang, S. Y.; Kim, S. W.; Oh, S. J.; Cho, J.; Pae, A. N.; Lee, C. J.; Park, K. D. Newly developed reversible MAO-B inhibitor circumvents the shortcomings of irreversible inhibitors in Alzheimer's disease. *Sci. Adv.* **2019**, *5*, No. eaav0316.

(5) Tzvetkov, N. T.; Stammler, H. G.; Neumann, B.; Hristova, S.; Antonov, L.; Gastreich, M. Crystal structures, binding interactions, and ADME evaluation of brain penetrant N-substituted indazole-5-carboxamides as subnanomolar, selective monoamine oxidase B and dual MAO-A/B inhibitors. *Eur. J. Med. Chem.* **2017**, *127*, 470−492.

(6) Tong, J.; Rathitharan, G.; Meyer, J. H.; Furukawa, Y.; Ang, L. C.; Boileau, I.; Guttman, M.; Hornykiewicz, O.; Kish, S. J. Brain monoamine oxidase B and A in human parkinsonian dopamine deficiency disorders. *Brain* **2017**, *140*, 2460−2474.

(7) Dezsi, L.; Vecsei, L. Monoamine oxidase B onhibitors in Parkinson's disease. *CNS Neurol. Disord.: Drug Targets* **2017**, *16*, 425−439.

(8) Guglielmi, P.; Carradori, S.; Ammazzalorso, A.; Secci, D. Novel approaches to the discovery of selective human monoamine oxidase-B inhibitors: is there room for improvement? *Expert Opin. Drug Discovery* **2019**, *14*, 995−1035.

(9) Gaspar, A.; Silva, T.; Yanez, M.; Vina, D.; Orallo, F.; Ortuso, F.; Uriarte, E.; Alcaro, S.; Borges, F. Chromone, a privileged scaffold for the development of monoamine oxidase inhibitors. *J. Med. Chem.* **2011**, *54*, 5165−5173.

(10) Reis, J.; Cagide, F.; Chavarria, D.; Silva, T.; Fernandes, C.; Gaspar, A.; Uriarte, E.; Remiao, F.; Alcaro, S.; Ortuso, F.; Borges, F. Discovery of new chemical entities for old targets: insights on the lead optimization of chromone-based monoamine oxidase B (MAO-B) inhibitors. *J. Med. Chem.* **2016**, *59*, 5879−5893.
(11) Fonseca, A.; Reis, J.; Silva, T.; Matos, M. J.; Bagetta, D.; Ortuso, F.; Alcaro, S.; Uriarte, E.; Borges, F. Coumarin versus chromone monoamine oxidase B inhibitors: quo vadis? *J. Med. Chem.* **2017**, *60*, 7206−7212.
(12) Alcaro, S.; Gaspar, A.; Ortuso, F.; Milhazes, N.; Orallo, F.; Uriarte, E.; Yanez, M.; Borges, F. Chromone-2- and −3-carboxylic acids inhibit differently monoamine oxidases A and B. *Bioorg. Med. Chem. Lett.* **2010**, *20*, 2709−2712.
(13) Reis, J.; Manzella, N.; Cagide, F.; Mialet-Perez, J.; Uriarte, E.; Parini, A.; Borges, F.; Binda, C. Tight-binding inhibition of human monoamine oxidase B by chromone analogs: a kinetic, crystallographic, and biological analysis. *J. Med. Chem.* **2018**, *61*, 4203−4212.
(14) Fonseca, A.; Matos, M. J.; Reis, J.; Duarte, Y.; Gutiérrez, M.; Santana, L.; Uriarte, E.; Borges, F. Exploring coumarin potentialities: development of new enzymatic inhibitors based on the 6-methyl-3-carboxamidocoumarin scaffold. *RSC Adv.* **2016**, *6*, 49764−49768.
(15) Gupta, S.; Ghosh, P.; Dwivedi, S.; Das, S. Synthesis of 6-aryl substituted 4-quinolones via Suzuki cross coupling. *RSC Adv.* **2014**, *4*, 6254−6260.
(16) Hadida, S.; Van Goor, F.; Zhou, J.; Arumugam, V.; McCartney, J.; Hazlewood, A.; Decker, C.; Negulescu, P.; Grootenhuis, P. D. Discovery of N-(2,4-di-tert-butyl-5-hydroxyphenyl)-4-oxo-1,4-dihydroquinoline-3-carboxamide (VX-770, ivacaftor), a potent and orally bioavailable CFTR potentiator. *J. Med. Chem.* **2014**, *57*, 9776−9795.
(17) Mesiti, F.; Maruca, A.; Silva, V.; Rocca, R.; Fernandes, C.; Remiao, F.; Uriarte, E.; Alcaro, S.; Gaspar, A.; Borges, F. 4-Oxoquinolines and monoamine oxidase: when tautomerism matters. *Eur. J. Med. Chem.* **2021**, *213*, 113183.
(18) Gomes, L. R.; Low, J. N.; Borges, F.; Gaspar, A.; Mesiti, F. The synthesis, crystal structure and Hirshfeld analysis of 4-(3,4-dimethylanilino)-N-(3,4-dimethylphenyl)quinoline-3-carboxamide. *Acta Crystallogr., Sect. E: Crystallogr. Commun.* **2020**, *76*, 201−207.
(19) Cecchetti, V.; Fravolini, A.; Fringuelli, R.; Schiaffella, F.; Lorenzini, M. C.; Tabarrini, O. 4H-1-benzothiopyran-4-one-3-carboxylic acids and 3,4-dihydro-2H-isothiazolo[5,4-bbenzothiopyran-3,4-diones as quinolone antibacterial analogs. *J. Heterocycl. Chem.* **1993**, *30*, 1143−1148.
(20) Wentland, M. P.; Lesher, G. Y.; Reuman, M.; Gruett, M. D.; Singh, B.; Aldous, S. C.; Dorff, P. H.; Rake, J. B.; Coughlin, S. A. Mammalian topoisomerase II inhibitory activity of 1-cyclopropyl-6,8-difluoro-1,4-dihydro-7-(2,6-dimethyl-4-pyridinyl)-4-oxo-3-quinolinecarboxylic acid and related derivatives. *J. Med. Chem.* **1993**, *36*, 2801−2809.
(21) Chavarria, D.; Fernandes, C.; Silva, V.; Silva, C.; Gil-Martins, E.; Soares, P.; Silva, T.; Silva, R.; Remiao, F.; Oliveira, P. J.; Borges, F. Design of novel monoamine oxidase-B inhibitors based on piperine scaffold: structure-activity-toxicity, drug-likeness and efflux transport studies. *Eur. J. Med. Chem.* **2020**, *185*, 111770.
(22) Chavarria, D.; Cagide, F.; Pinto, M.; Gomes, L. R.; Low, J. N.; Borges, F. Development of piperic acid-based monoamine oxidase inhibitors: synthesis, structural characterization and biological evaluation. *J. Mol. Struct.* **2019**, *1182*, 298−307.
(23) Bonifácio, M. J.; Vieira Coelho, M. A.; Soares da Silva, P. c. Kinetic inhibitory profile of BIA 3-202, a novel fast tight-binding, reversible and competitive catechol-O-methyltransferase inhibitor. *Eur. J. Pharmacol.* **2003**, *460*, 163−170.
(24) Dharmasena, S. P.; Wimalasena, D. S.; Wimalasena, K. A slow-tight binding inhibitor of dopamine beta-monooxygenase: a transition state analogue for the product release step. *Biochemistry* **2002**, *41*, 12414−12420.
(25) Clark, D. E. Rapid calculation of polar molecular surface area and its application to the prediction of transport phenomena. Prediction of blood-brain barrier penetration. *J. Pharm. Sci.* **1999**, *88*, 815−821.
(26) Chen, N.; Song, Z. M.; Tang, H.; Xi, W. S.; Cao, A.; Liu, Y.; Wang, H. Toxicological effects of Caco-2 cells following short-term and long-term exposure to Ag nanoparticles. *Int. J. Mol. Sci.* **2016**, *17*, 974.
(27) Kanat, O. N.; Selmanoglu, G. Neurotoxic effect of Fipronil in neuroblastoma SH-SY5Y cell line. *Neurotoxic. Res.* **2019**, *37*, 30−40.
(28) Sidell, N. Retinoic acid-induced growth inhibition and morphologic differentiation of human neuroblastoma cells in vitro. *J. Natl. Cancer Inst.* **1982**, *68*, 589−596.
(29) Kovalevich, J.; Langford, D. Considerations for the use of SH-SY5Y neuroblastoma cells in neurobiology. *Methods Mol. Biol.* **2013**, *1078*, 9−21.
(30) Fernandes, C.; Martins, C.; Fonseca, A.; Nunes, R.; Matos, M. J.; Silva, R.; Garrido, J.; Sarmento, B.; Remião, F.; Otero-Espinar, F. J.; Uriarte, E.; Borges, F. PEGylated PLGA nanoparticles as a smart carrier to increase the cellular uptake of a coumarin-based monoamine oxidase B inhibitor. *ACS Appl. Mater. Interfaces* **2018**, *10*, 39557−39569.
(31) Repetto, G.; del Peso, A.; Zurita, J. L. Neutral red uptake assay for the estimation of cell viability/cytotoxicity. *Nat. Protoc.* **2008**, *3*, 1125−1131.
(32) Moraes, C. B.; Witt, G.; Kuzikov, M.; Ellinger, B.; Calogeropoulou, T.; Prousis, K. C.; Mangani, S.; Di Pisa, F.; Landi, G.; Iacono, L. D.; Pozzi, C.; Freitas-Junior, L. H.; Dos Santos Pascoalino, B.; Bertolacini, C. P.; Behrens, B.; Keminer, O.; Leu, J.; Wolf, M.; Reinshagen, J.; Cordeiro-da-Silva, A.; Santarem, N.; Venturelli, A.; Wrigley, S.; Karunakaran, D.; Kebede, B.; Pohner, I.; Muller, W.; Panecka-Hofman, J.; Wade, R. C.; Fenske, M.; Clos, J.; Alunda, J. M.; Corral, M. J.; Uliassi, E.; Bolognesi, M. L.; Linciano, P.; Quotadamo, A.; Ferrari, S.; Santucci, M.; Borsari, C.; Costi, M. P.; Gul, S. Accelerating drug discovery efforts for trypanosomatidic infections using an integrated transnational academic drug discovery platform. *SLAS Discovery* **2019**, *24*, 346−361.
(33) Liu, Q.; Hou, J.; Chen, X.; Liu, G.; Zhang, D.; Sun, H.; Zhang, J. P-glycoprotein mediated efflux limits the transport of the novel anti-Parkinson's disease candidate drug FLZ across the physiological and PD pathological in vitro BBB models. *PLoS One* **2014**, *9*, No. e102442.
(34) Bicker, J.; Alves, G.; Fortuna, A.; Falcao, A. Blood-brain barrier models and their relevance for a successful development of CNS drug delivery systems: a review. *Eur. J. Pharm. Biopharm.* **2014**, *87*, 409−432.
(35) Miller, D. S.; Bauer, B.; Hartz, A. M. Modulation of P-glycoprotein at the blood-brain barrier: opportunities to improve central nervous system pharmacotherapy. *Pharmacol. Rev.* **2008**, *60*, 196−209.
(36) Gameiro, M.; Silva, R.; Rocha-Pereira, C.; Carmo, H.; Carvalho, F.; Bastos, M. L.; Remiao, F. Cellular models and in vitro assays for the screening of modulators of P-gp, MRP1 and BCRP. *Molecules* **2017**, *22*, 600.
(37) McCaffrey, G.; Staatz, W. D.; Sanchez-Covarrubias, L.; Finch, J. D.; Demarco, K.; Laracuente, M. L.; Ronaldson, P. T.; Davis, T. P. P-glycoprotein trafficking at the blood-brain barrier altered by peripheral inflammatory hyperalgesia. *J. Neurochem.* **2012**, *122*, 962−975.
(38) Reichert, C. O.; de Freitas, F. A.; Sampaio-Silva, J.; Rokita-Rosa, L.; Barros, P. L.; Levy, D.; Bydlowski, S. P. Ferroptosis mechanisms involved in neurodegenerative diseases. *Int. J. Mol. Sci.* **2020**, *21*, 8765.

https://doi.org/10.1021/acs.jmedchem.1c00510
J. Med. Chem. 2021, 64, 11169−11182